CODEN:LUTEDX/(TEIE-5378)/1-81(2016)

Electrical Engineering and Automation

Industrial

Ultrasonic Positioning System for Electric Road

Robin Hedlund

Marcus Romner

Division of Industrial Electrical Engineering and Automation
Faculty of Engineering, Lund University

Ultrasonic Positioning System for Electric Road System

Faculty of Engineering, Lund University

Industrial Electrical Engineering and Automation

Robin Hedlund, Marcus Romner

Supervisor: Gunnar Lindstedt, Associate Professor
Examiner: Mats Alaküla, Professor

October 7, 2016

Abstract

Elonroad is a company that is looking into the possibility to charge electric vehicle on road. The conductor implemented on the driveway has a characteristic shape. The scope of this master thesis project is to identify the shape of the conductor and determine the relative position of the vehicle to the conductor using ultrasonic sensors. The goal is to have an update frequency of 30 Hz and a positioning error of maximum 2 cm. During the project a serial system containing 7 ultrasonic modules has been built. The sensor modules are mounted in an array and placed parallel to the road and perpendicular to the vehicles intended direction of travel. The ultrasonic modules are placed with a center distance of 10 cm on the array. A cross-correlation algorithm was implemented to determine the distance to the surface below each of the ultrasonic modules. The method to find the relative position of the vehicle uses a modified convolution algorithm which is proven to work under ideal circumstances. The distance measurement from the modules to ground can differ roughly +/-8 mm, this originates from the wavelength of the 40 kHz ultrasonic signal in air, the +/-8 mm error can, according to simulations give a positioning error of up to 5 cm. Simulations has indicated that +/-4 mm will give a positioning error less than, or equal to, 2 cm. The update frequency is assumed to be around 20 Hz, where the largest part is due to calculation time of the distance to ground. It can be lowered with more effective algorithms or with a more powerful microcontroller.

Preface

The master thesis project has been very educative at several levels for us, using tools and techniques that was for us, unheard of before the project started. The project has combined physics, hardware design, software implementation and signal processing in an interesting and educative way. Both participants has contributed equally to this thesis and worked together with all parts of the project.

The project would not have come as far if it was not for the staff of the department of Industrial Electrical Engineering and Automation. Our supervisor Gunnar Lindstedt, project leader Dan Zethraeus, our examiner Mats Alaküla, research engineer Getachew Darge for unbearable help in the laboratory, we are very grateful for their help and also to others who have helped us throughout the project.

Last but not least we would like to thank our friends and family whom had patience with us during the long days of the project.

1 Abbreviations

ADC	Analog to Digital Converter
AM	Amplitude Modulation
CAD	Computer Aided Drawing
CPU	Central Processing Unit
DFT	Discrete Fourier Transform
DIN	German Institute for Standardization
DMA	Direct Memory Access
D-SUB	D-Subminiature
EMC	Electromagnetic Compatibility
ERS	Electric Road System
FFT	Fast Fourier Transform
FHSS	Frequency Hopping Spread Spectrum
FM	Frequency Modulation
I^2C	Inter-Integrated Circuit
IC	Integrated Circuit
IDE	Integrated Development Environment
IEEE	Institute of Electrical and Electronics Engineers
IFFT	Inverse Fast Fourier Transform
MCU	Microcontroller Unit
Msps	Mega samples per second
Op amp	Operational Amplifier
PCB	Printed Circuit Board
PSU	Power Supply Unit
PWM	Pulse Width Modulation
RAM	Random Access Memory
SCL	Serial Clock
SDA	Serial Data
SMD	Surface Mounted Device
ToF	Time of Flight
UART	Universal Asynchronous Receiver/Transmitter
UPS	Ultrasonic Positioning System
USART	Universal Synchronous/Asynchronous Receiver/Transmitter
USB	Universal Serial Bus
UV	Ultra Violet

Contents

2 Introduction

2.1 Background

The European Union has set a goal that the carbon emissions shall be reduced with 80-95 % to 2050, from 1990 levels. In Sweden the parliament has accepted the goal and a vision that to 2050 not have any net emissions of greenhouse gases. Sweden has gone even further and added a target to have a vehicle fleet that is independent of fossil fuels by 2030. This pushes the development of the vehicle industry to new levels and technical solutions. [1]

As a step in this the department of Industrial Electrical Engineering and Automation (IEA) collaborates with the recently founded company Elonroad to develop an electric road system (ERS) that will allow charging of electric vehicles on road. The part of the system integrated with the road surface consist in an elevated structure on the driveway. The key element of the concept is that the elevation is possible to add to existing road without breaking the asphalt. The elevated structure consists of ramps on both sides with an electric conductor in the intersection. The power conductor is seen as a flat surface on the top of the driveway structure. The power transfer between the conductor and the vehicles are made through sliding contacts. The sliding contacts are attached to a pick-up, a sort of sledge that is able to move vertically and sideways relative to the vehicles direction of travel. The pick-up is mounted underneath the vehicle. There is only one conductor on the road, the conductor on the roadway switches electric potential on small sections as the car moves forward along the road and the vehicle is connected with several sliding contacts.

Elonroad has received fundings from the Swedish energy authority (Swe: Energimyndigheten) to further investigate the realization of the ERS project.

To establish a connection to the conductor on the roadway, some sort of sensors is required to give a positioning of the car relatively the conductor. Since a strong current travels through the road conductor, it is tempting to use inductive sensors. However, there are several competitors currently using inductive sensors and there are no other players in the market with the elevated shape that Elonroad are looking in to, which gives Elonroad a unique opportunity. Several of the other available sensor types are either too inaccurate, too expensive or their functions are drastically degraded by dust and dirt. Positioning measurement using ultrasound could therefore be a good option if proven to work.

2.2 Scope

This project will look further into the possibility to use ultrasound to accurately determine a vehicles position using a stationary point of reference. During the project a literature study has been carried out focusing on ultrasound in general and applied use of ultrasound in particular. Tests and anal-

ysis of existing ultrasound parking sensors has been conducted, since these are tested products already available on the market and are customized for the strains sensors on a moving vehicle on road is put under. Since the idea is to put the measurement system in a commercial product, it is important to keep the cost of a possible future product low which limits the use of already existing ultrasound distance measure sensors.

To be able to connect to the conductor in the road, the initial goal was to have an accuracy of 20 mm and an update frequency of 30 times per second. In order to determine the position of the road elevation accurately relative to the car, it is a necessity to have a high and reliable measurement of the distance from underneath the car to the ground beneath each of the ultrasound sensors.

A system has been built during the project, consisting of an arbitrary number of ultrasound distance measurement nodes. The different distances provided from the nodes is compiled to give a relative position to the road elevation.

The measurement distance error between the sensor and the ground need to be as small as possible. This error risks to be translated to the calculated relative distance of the road elevation and thereby give false data of the vehicles relative position.

The final goal was to design and develop a prototype that would be tested under real conditions performing measurements from under a moving vehicle, this was only if there was time left in the project.

2.3 Projects Unique use of Ultrasound Sensors

Ultrasound is today well investigated and much research and development has been conducted in the area. But ultrasound is a large subject and most of the research has been focused on the medical fields use of ultrasound. Ultrasound sensors are today mostly used for measurements in fluids and solid materials while the area of use in air is fairly limited. The goal that this project is focusing on, to determine a vehicles position relatively a stationary known structure in the roadway (Figure 1), is as far as known, a completely new field for ultrasound.

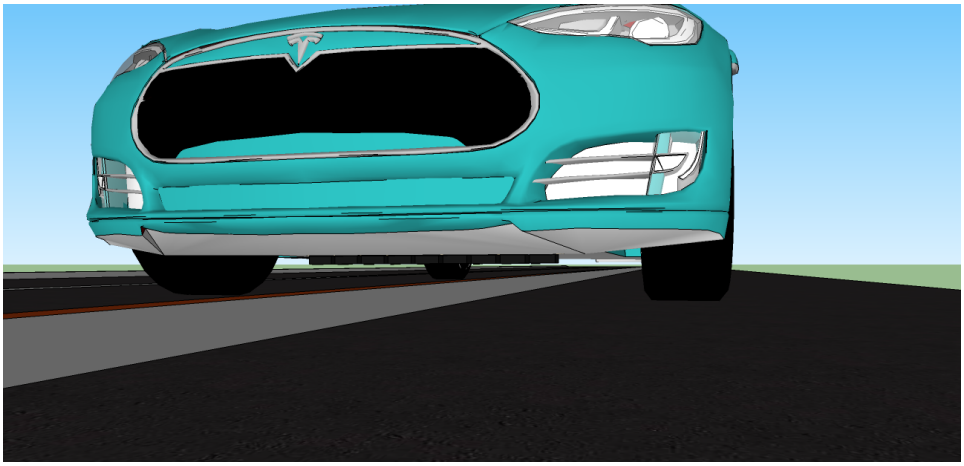

Figure 1: *The projects concept with a sensor array to locate the electric road.*

2.4 Elonroad and Competetive Existing Systems

Except Elonroad there are other companies working on developing an ERS. There are three other major competing systems that are being developed. They are using other possible sensing technologies than ultrasound to find the road part of the ERS. Mainly there are two other sensing methods possible, which are inductive sensing of the electric field in the road and visual feedback from a camera.

2.4.1 Elonroad

Elonroad's concept is to add the electric road on top of the existing driveway. This will cause a small elevation in the middle of the road. The shape of the electric road is a triangle with a flat top, where the flat top is the conductor. There is only a single conductor, which switches electric potential in the direction of travel. The conductor is divided into segments which can be turned on and off so that the road is only powered when there is a vehicle connected to it. A pick-up under the vehicle transfers power from the road. The pick-up can move sideways to let the vehicle move laterally without loosing the connection to the conductor [2]. A big challenge is to find where the conductor is relative to the vehicle so that the pick-up can move to the right position without loosing connection. This project is looking into possibilities of doing this by using ultrasound. Elonroad's concept can be seen in Figure 2.

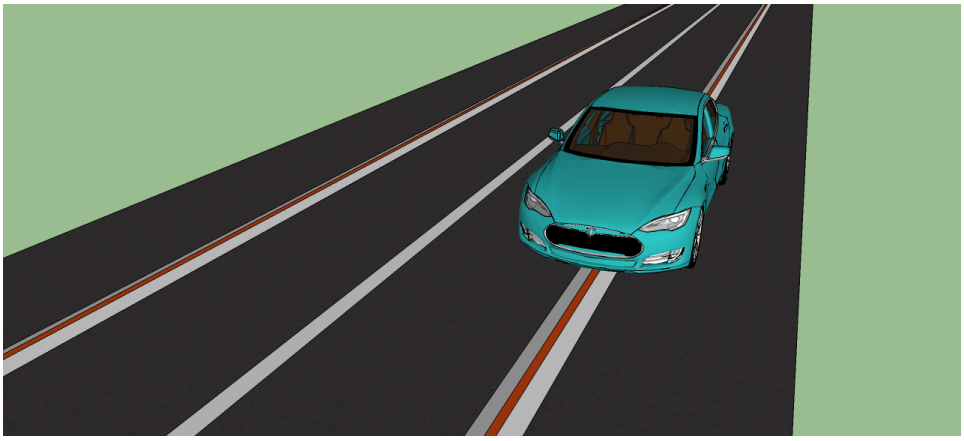

Figure 2: *Elonroad's concept with an elevated road structure.*

2.4.2 Siemens eHighway

Siemens are developing a concept that allows trucks and buses to charge their batteries and drive from the electric grid through overhead lines. The trucks will use pantographs just as trains to transfer power. They already have a test site in Germany and will probably be the first to have a test section in the world, either in California or at E16 outside Gävle in Sweden. Siemens collaborates with Scania trucks with the development of the system [3] [4]. The largest drawback with this system are the limitations that only heavy traffic such as trucks and buses can utilize it. One advantage of the system is that it is tested and used in the train and tram industry. Another advantage could be less cleaning than a system that lies in the ground.

Figure 3: *Siemens concept eHighway with overhead lines. [5]*

2.4.3 Elways

Elways is similar to Elonroad as both uses conductive transfer of power from a rail in the road. The largest difference is that Elways track is submerged in the asphalt but Elonroad lays on the top of the road. Another difference is that Elways pick-up follows the track mechanically when it is connected because of its U-beam design of the submerged track. This means that they only have to find the road part of the ERS once to connect. This design is positive in the way that it does not have to actively search for and find the way, but it could have big problems with dirt in the U-beam track and with mechanical issues such as wear. To find the track in the road Elways uses inductive sensing on the pick-up and sweeps for the road part. One big advantage with inductive sensing over ultrasonic measurements is that it has already been proven to work, but this then comes with a higher cost because they are already patented by other companies. The inductive sensor could be disturbed by the electric transfer from the road to the vehicle, especially with sparks that could occur. This is not a problem for Elways since they only search for the electric way before they connect to it but could be a challenge for Elonroad [6].

Figure 4: *Elways concept with tracks milled into the asphalt. [7]*

2.4.4 Alstom and Volvo

Alstom and Volvo are developing a test track with conductive power transfer mainly developed for trucks. The system uses two powerlines in the ground and have an electric pick-up for power transfer. They control the pick-up actively after positioning from an inductive sensor which detects where the electric power lines are [8].

Figure 5: *Volvo and Alstom's concept for the ERS. [8]*

2.5 Resources

To implement this master thesis project, there was a local lab at the projects disposal. There has also been free access to tools, waste materials and standard electrical components during the project. The lab was provided

by IEA in the departments areas. A small 3D printer has been available in the lab throughout the project. A workshop for etching PCBs has also been available when required.

An initial budget of 5,000 SEK was set for the project. The money was mainly used for purchasing components. The project was financed by Elonroad. A small sample of the shape of the electric road was available for tests.

The computers used throughout the project has been private and from the undersigned's providence.

3 Ultrasound

3.1 Introduction

Ultrasound is defined as sound with a frequency above the human hearing range. In other words, sound with a frequency higher than 20 kHz. In a physical point of view there is no difference between ultrasound and audible sound apart from the different characteristics of the higher frequencies. [9]

The credit for discovering ultrasound diverge depending who you ask, but biologist Lazzaro Spallanzani from Italy demonstrated in 1794 bats ability of navigating in the dark with echo reflection from high frequency inaudible sound. [10]

3.2 Physics

Since the physics behind ultrasound is the same as for sound, this means that the theory of acoustics which is a mechanical energy is applicable. Ultrasound is sound waves and are known as both acoustic and elastic waves [11]. In air, sound waves are fast changes in pressure difference created by a moving or vibrating object. When an object moves forward it pushes the air in front of it which is then compressed. When the object then moves backwards it instead decompresses the air [12, chapter 15, p.496]. This causes a wave of pressure which propagates adiabatically and longitudinally, the further the wave travels the more it attenuates. The same phenomena can be seen on water, when an object is dropped into water it creates a wave that propagates through the water until it eventually has too small amplitude to be distinguished. How big the pressure difference is, relates to the amplitude or the intensity of the wave, this is experienced as volume of the sound. The pitch of the sound depends on how fast the object is moving back and forth, which is called frequency. The frequency is measured in Hertz which means how many times the objected has moved back and forth over one second. [13]

The propagation velocity for a soundwave in air is dependent of factors such as temperature, humidity and air pressure. The velocity can be calculated according to Equation 1. The propagation velocity for air with a temperature of 20 °C is 343 m/s.

$$v = \sqrt{\frac{\gamma * RT}{M}} \tag{1}$$

Where v is velocity in the gas. T is the absolute temperature in Kelvin, γ is a dimensionless constant. γ has for diatomic atoms the value 7/5 and since air to 98 % consists of O_2 and N_2, this is the value used for velocities in air. R is the universal gas constant 8.3145 $J/(M * K)$ and M is the mass

of one mole of the gas, for air $M = 29.0 * 10^{-}3\ Kg/Mol$. [12, chapter 15, p.499]

The ultrasound measurements are made by sending an electric pulse to an ultrasound transducer which then emits a soundwave. By listening to the echo from the soundwave and measuring the Time of Flight (ToF) between the first pulse and the echo it is possible to determine distance to the points where the sound wave reflexes. The reflecting sound can be measured by either the same transducer that emitted the ultrasound or by other transducer/transducers. In some applications it is enough to just listen to the first echo, this will allow measurement to the first object. In most applications however, it is of interest to listen to several echoes in order to create a visualization over the measured object or area. To measure several objects in an area, several samples or pings are required from different positions or different angles.

3.2.1 Ultrasonic Transducer

To generate ultrasound for measurement a transducer is used. A transducer is a device that transform one form of energy into another. In this project the transducer transforms electric energy into mechanical energy, which emits a soundwave. The transducer also works the other way around where it transforms mechanical energy into electrical energy.

The ultrasonic transducers are commonly made out of one of two different technologies, either piezoelectric or electrostatic. It is common for a transducer to emit a wide range of frequencies. Depending on the damping factor in the transducer, the frequency span in the emitted bandwidth is varied. For a transducer with a higher damping factor the emitted signal consists of a wider bandwidth and a shorter pulse than a transducer with a lower damping factor. [14, chapter 8]

3.2.2 Piezoelectric transducer

The piezo-electric effect was discovered by Pierre Curie and his brother Jacques Curie in Paris, France 1880. They observed that when mechanical pressure was exerted on a quartz crystal, an electric potential was produced. The first application was an underwater sonar detection system both used to find icebergs after the Titanic disaster and also to navigate under water and to find submarines in World War I. [10]

A piezoelectric transducers core, or the active element, consists of a constant polarized element. When an electric field is applied over the element the polarized molecules will align with the electric field and thereby cause a change in physical dimension. When mechanical force instead is applied to the element it will produce an electric field. The polarity of the field depends on the direction of the force, which means that an alternating current (AC)

is generated. This allows both detection and transmission of ultrasound waves. [15, chapter 1.2] [16]

The core element is today most often made out of a ceramic wafer and depending on the physical dimensions of the wafer, the resonant frequency can be varied. A thinner wafer produces an ultrasound of higher frequency as compared to a thicker wafer. [17]

3.2.3 Electrostatic Transducer

An electrostatic transducer consists of 3 components, a thin diaphragm, spacers and 2 stators. The diaphragm is usually made out of plastic and is coated with an electrically conductive material or in the case of ultrasonic transducers made of silicon. It is suspended between the 2 stators with help of the spacers to make a small air gap. The stators are made of electrically conductive grids, such as perforated steel sheets coated with an insulator. The stators are perforated to let the sound pass through them. A constant charge is applied to the diaphragm, while the stators are driven by an AC signal. This causes a uniform electrostatic field proportional to the AC signal between the stators which makes the diaphragm move back and forth. The electrostatic transducer can also be made out of 1 stator instead of 2, this causes the diaphragm to get a non-linear behavior causing harmonic distortion. Since the electrostatic transducer has no closed circuit it is in effect a capacitor and is therefore voltage driven. This means that it needs an impedance matching transformer to be driven from a normal amplifier. [18]

The electrostatic transducer has a wider bandwidth compared to the piezoelectric. It is harder to protect the diaphragm from dirt and external influences and is also a more expensive solution as compared to the piezoelectric transducer.

3.3 Areas of Use

There are several fields where ultrasound measurements are used, it has advantages over other comparable methods where it is non-destructive and there are no evidence that it would be hazardous for nearby personnel. It can be a contact less measurement method. [13]

3.3.1 Medical

The medical sector uses ultrasonic in several different areas to look at tissues and internal body structures. Medical ultrasound is called diagnostic sonography and it uses imaging technique with ultrasound to build a picture of the tissue/structure. The speed of sound in liquids is 4.3 times faster than in air resulting in longer wavelengths, therefore diagnostic sonographic scanners operate in a high frequency range between 2-18 MHz. The frequency sets the resolution and penetration depth, higher frequency gives higher

resolution but lower depth and vice versa. The most common ultrasound application people think about is probably obstetric ultrasound, which is the practice of examining a fetus inside a pregnant woman. There are also a lot of other applications, for example with the help of Doppler effect (Section 4.7) it is possible to calculate and visualize the blood flow. There are many advantages with sonography compared to other methods such that it can be made small and portable, it renders real-time live images and it has no known long-term side effects. [19] [16]

3.3.2 Measurements in Solid Materials

Measurement made in solid materials with ultrasonic sound allows a non-destructive method to find irregularities within the material. It is thereby possible to, for example, find cracks and cavities in steel beams which could otherwise be devastating since they would weaken the construction. Ultrasound is also used for material characterization, inspection and can measure the thickness of materials and delamination. There are several methods used for the nondestructive measurements, such as resonance method and pulse-echo. Different frequency's are used depending on material and grain size. [13, chapter 7]

3.3.3 Other uses

Ultrasound gives rise to cavitation in liquids, therefore ultrasound has been a great help when studying cavitation. When the cavitation bubbles collapses they give rise to shock waves, this is used in cleaning processes to shake particles off.

Tools that vibrates with ultrasound makes it possible to solder or weld materials that cannot be handled with conventional methods, for example when soldering aluminium the ultrasonic vibrations tear off the oxide layer which otherwise prevents the solder to adhere.

Ultrasound can also be used for level measurement in tanks and distance measurements. [9]

3.3.4 Ultrasound in Nature

Ultrasound is utilized by some mammals and birds, mainly for echolocation and communication. Bats utilizes ultrasound for navigation and to find prey in the dark. The bats emit sound bursts of 11-212 kHz depending on species, most bats call with frequencies between 20 kHz and 60 kHz. When the bat is hunting they produce 10 sound pulses per second and as they are closing into the prey they increase the rate of pulses up to as high as 200 pulses per second. This is because bats emit the next pulse immediately after hearing the echo from the prey. The length of the call duration (pulses) is also reduced to avoid signal overlap between the emitted sound and echo

when the bat closes in. Different species have developed different abilities depending on environment and therefore emits pulses at different rates, bats flying in open air for example emits longer pulses with longer pulse interval. This slows down the update rate of the acoustic image and therefore some bats can even change their call type, so they can address different echoes. [20]

Toothed whales and dolphins can hear and produce ultrasound, they use it for navigation, communication and even to stun and capture prey. Dogs can also hear ultrasound and there are whistles for dogs that produce ultrasound. [9]

Approximate data for some different animals hearing range is displayed in Table 1, of course there exists a lot of other animals that are not mentioned here which can hear in the ultrasound range.

Animal	**Frequency [Hz]**
Bat	11 000-212 000
Cat	45-64 000
Cattle	23-35 000
Dog	67-45 000
Dolphin	150-150 000
Horse	55-33 500
Human	20-20 000
Mouse	1000-91 000
Rabbit	360-42 000
Rat	200-76 000

Table 1: *Hearing range for different animals. [21]*

4 Theoretical Background

4.1 Threshold Detection

The threshold detection method is relatively simple; it measures the amplitude of the returning signal from a pulse echo. If the amplitude exceeds a pre-set threshold value the detection has occurred. This method can be implemented relatively simple on a microcontroller unit (MCU) with an external comparator that trigs the MCU when the threshold is exceeded. The threshold can also be defined internally in the MCU that an anlog to digital conversion (ADC) sampled value is compared to. The drawback with threshold detection is that the first fraction of the signal has already started to rise when the threshold is exceeded.

The limitation of this method is due to background noise which can exceed the threshold value even before the signal of interest occurs, which is why it is not possible to set the threshold as low as it needs to be, to be sufficient for the application intended in this projects final stage. A threshold detection would at best tune give a resolution error of a few millimeters, which is what the manufacturer of sensors on the market specifies.

4.2 Cross-Correlation Using Cooley-Tukey FFT Algorithm

The algorithm used for fast Fourier transform on the microcontroller is Cooley-Tukey FFT. This is the most used FFT algorithm due to its relatively simplicity and efficiency [22]. Originally the algorithm was first described by Carl Fredrich Gauss in 1805, which contained the factorization steps of the algorithm [23]. The FFT algorithm was made famous when J. Cooley and J. Tukey published the article *An algorithm for the machine calculation of complex Fourier series* in 1965 of how to use discrete Fourier transform efficiently [24]. The variant of the algorithm which is used in this project is called radix-2, which is the simplest and most commonly used variant of the Cooley-Tukey algorithm. The algorithm gains its fast speed from reusing already calculated intermediate computations.

$$X_k = \sum_{n=0}^{N-1} x_n e^{-\frac{2\pi i k n}{N}} \tag{2}$$

Discreet Fourier transform (DFT) is defined as Equation 2 where the transferred array $X = [X_0 \dots X_{N-1}]$ and $k \epsilon [0, N-1]$.

DFT requires $\mathcal{O}(n^2)$ operations since there for every k is N number of n which each requires N complex multiplications and N-1 additions. A fast Fourier transform requires only $\mathcal{O}(n \log_2 n)$ operations if N is a power of 2. The key to decrease the number of operations is to reuse already calculated values. By rewriting Equation 2 into Equation 3 two sequences

of length N/2 where the first sequence sums even numbers and the second odd numbers. Let $W_N^k = e^{-\frac{2\pi ikn}{N}}$ and use the connection $W_N^2 \Leftrightarrow W_{N/2}$ since $e^{-\frac{2\pi ikn}{N}*2} \Leftrightarrow e^{-\frac{2\pi ikn}{N/2}}$ and break out W_N^k from the odd expression.This is known as Danielson-Lanczos Lemma. [25]

$$X_k = \sum_{n=0}^{N/2-1} x_{2n} W_{N/2}^{kn} + W_N^k \sum_{n=0}^{N/2-1} x_{2n+1} W_{N/2}^{kn} \tag{3}$$

The number of calculations required are now $N^2/2+N$ which is roughly half of what DFT uses. The trick with radix-2 is that it is possible to recursively remake the step above. If x contains 2^p number of elements, the step can be remade p times. And finally the operations required are $N^2/N+Nlog2(N)$ or $\mathcal{O}(N \log_2 N)$. Another trick to reduce the total number of computations further by a factor of 2 is to use the periodicity that $X_k = E_k+W_N^k O_k$ and $X_{(k+N/2)} = E_k-W_N^k O_k$ where E is the sum of even elements and O the sum of odd elements. Figure 6 shows a comparison of how efficient FFT is compared to DFT. [26]

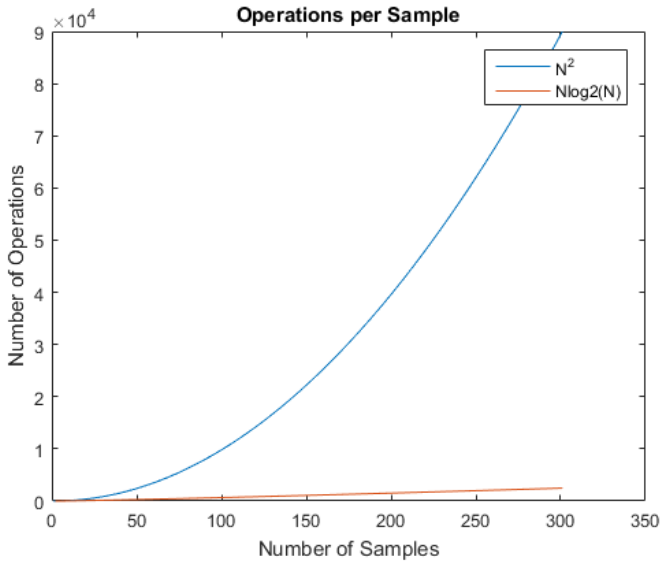

Figure 6: *Comparison between the number of operations required for DFT* $\mathcal{O}(n^2)$ *and FFT* $\mathcal{O}(n \log_2 n)$

Two series of data $x = [1\,1\,1]$ and $y = [1\,1\,1]$. In the time domain the cross correlation xy_{corr} between the series of data can be described as moving one of the series over the other and multiply each value and then take the sum for each position. The three first steps can be seen below, the resulting length of the result vector will be length(x)+length(y)-1.

```
[1 1 1]          [1 1 1]          [1 1 1]
    [1 1 1]          [1 1 1]          [1 1 1]
1*1=1        1*1+1*1=2        1*1+1*1+1*1=3
```

This yields the resulting vector $xy_{corr} = [1\,2\,3\,2\,1]$. As can be seen the largest value in the resulting vector corresponds to the best match of the data series, however this is not true for all cases.

Figure 7: *Example of correlation between two series of data in time domain.*

Cross-correlation in time domain can be seen in Figure 7. The cross-correlation in frequency domain is performed by transforming both arrays and element-wise multiply them, where one of the arrays is complex conjugated. Thereafter perform the inverse fast Fourier transform (IFFT). The inverse discrete Fourier transform is described in Equation 4. The steps to rewrite this equation to IFFT is the same as for FFT from DFT. The 1/N in the IFFT is not necessary to perform since this only is a scale factor and can thereby be excluded reduce the number of operations.

$$X_k = \frac{1}{N} \sum_{n=0}^{N/2-1} x_{2n} e^{+\frac{2\pi i k n}{N}} \tag{4}$$

The equation for cross-correlation in frequency domain using Fourier transforms can be written as Equation 5.

$$x \star y = \mathcal{F}^{-1}\big(\mathcal{F}(x) \circ \overline{\mathcal{F}(y)}\big) \tag{5}$$

where x and y are the data input arrays. $\mathcal{F}$ is the FFT, $\mathcal{F}^{-1}$ represent the IFFT. $\circ$ is element-wise multiplication and the overline is complex conjugate. The length of the resulting array will be the length of the combined number of elements in the cross-correlated arrays minus 1.

One aspect to keep in mind when performing the cross-correlation in frequency domain is that when the data is inverse transformed it is shifted. So the values are dislocated in the resulting array and will be in the order shown in Equation 6.

$$W = [w_0, w_1, \ldots\, w_{N-1}, w_{-(N-1)}, w_{-(N-2)}, \ldots, w_{-1}] \tag{6}$$

assuming both arrays are of same length. The shift is due to a circular correlation has been performed and not a linear which would have been the case in time domain. This shift needs to either be considered when the cross-correlation is analyzed or the data points needs to be shifted into the correct order. To prevent this wrap around it is possible to pad the data with zeros.

In other words, the Cooley-Tukey algorithm increases the required memory to reduce calculation time as compared to time-domain cross-correlation.

4.3 Analog to Digital Conversion

An ADC is a technical component that translates an analog signal to a quantized digital value. The analog signal can originate from one of several sources, such as light, sound, voltage, acceleration or current. An ADC used in microcontrollers usually measures voltage. The microcontroller measures the signal by dividing a voltage span in a number of levels, the number of levels sets the resolution of the ADC. Typically the resolution is a multiple of 2 for example 8 bit, 10 bit, 12 bit etc. The Bandwidth of the ADC is defined primarily by its sampling rate. Therefore, the bandwidth can be used combined with the Nyquist-theorem to determine the theoretical maximum frequency of the sampled signal for it to be rendered in a correct way. [27, chapter 6]

Usually a sample and hold circuit is used to measure the level of a sample. When taking a sample, the ADC charges a capacitor with the voltage that should be measured. Thereafter the capacitors voltage is measured with a comparator bit by bit. The value of a sample is stored in the ADC, until a new sample is performed, see Figure 8. [28]

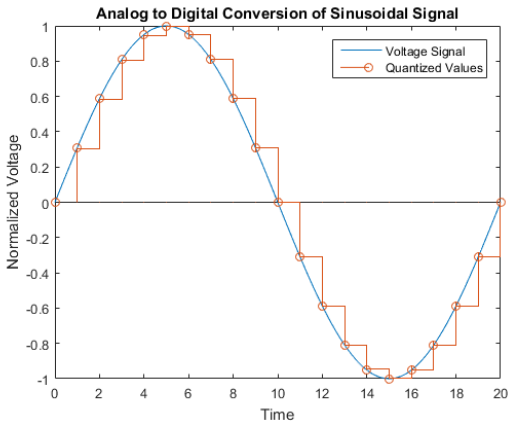

Figure 8: *Visual explanation behind the concept sample and hold ADC. This is how the ADC quantize an analog signal.*

In order to accurately represent the analog data, the sample clock needs to be evenly spaced in time. Any deviation of the clock will be translated to the sampled value and the data will be distorted. The deviations from the clock affects the most when the change in input voltage is as largest. In other words, when the derivative is at its highest value. [29]

4.4 I^2C Communication

I^2C (Inter-Intergrated Circuit) is a serial bus communication system. It was introduced by Philips Semiconductor in the early 1980s. Initially developed for microcontrollers to communicate with peripheral ICs on the same circuit board [30]. The I^2C protocol provides low support for error handling. If any error handling needs to be used, it has to be implemented by the user at high level programming. The communication bus uses two wires, one clock line and one serial data line. The wires are called SDA and SCL respectively. Both lines are open-drains connected via pull-ups to Vdd as shown in Figure 9.

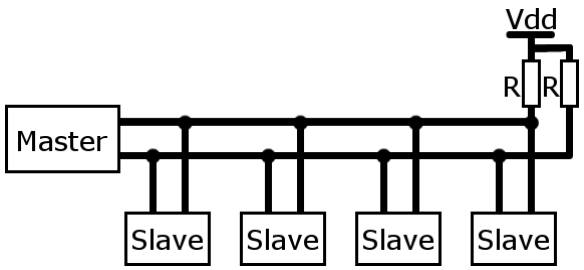

Figure 9: *A simplified I^2C bus system where 4 slaves are connected to a master using clock line and data line. The set up requires the master and the slave to share a common ground.*

The bus system is built with a master-slave hierarchy, where the master always initiates the communication. The master can either send data to the slave or request the slave to send data to the master. Each slave has its own unique 7 bit number saved in its address register. When an address is sent by the master, the slave compares it to the address register. See Figure 10 where the first 7 bits represents the address with most significant bit first. If the address matches the register, the slave replies with an acknowledgment. Then, depending on the value of bit number 8, either transmits data to the master or receives data from the master [31, p.335]. If the slave is for any reason not ready to reply to the master, it can stretch the clock by pulling the clock line low and thereby delaying the expected reply.

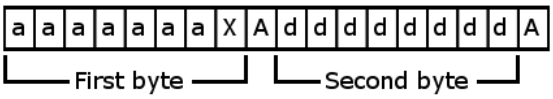

Figure 10: *I^2C initiated communication. Where a represents the 7 address bits, X is if the master want to read or write data, A is acknowledgment from the slave and d is the data transferred.*

The slaves can also listen to a broadcast which calls a common address for all slaves on the bus line, by default 0x00. A broadcast in I^2C is called a general call. This address can be used by the master to send data packets to all the slaves connected to the line simultaneously. Broadcast calls only reaches slaves set to read from the general call address. The master does not know how many slaves that are receiving the broadcast, as long as at least one slave acknowledges the address, the data will be transferred. [32]

4.5 UART Communication

UART is an abbreviation for Universal Asynchronous Receiver/Transmitter. The UART is a hardware with the transmitter that converts parallel data into serial data and thereafter transmit it to peripheral device. UART communication consists of one or more transmitter/receiver. The parallel to serial conversion is made by the use of a shift register, this allows data to be sent through a single wire, one bit at a time. The receiving device has a similar hardware device that shifts the data back in order and convert the bits back into parallel data. UART has full duplex communication, two wires to connect two devices, one wire for transmitting, and one for receiving data. This allows data to be transmitted and received simultaneously.

A UART message consists of 1 start bit, 5-9 data bits, typically 8, optionally a parity bit and one or two stop bits.

The commutation via UART is controlled by a clock signal that runs at a multiple of the data rate at all the devices connected on the lines. Unlike USART the UART devices has (usually) no shared clock signal. This means that the clocks of the transmitter and receiver needs to be synchronized during a transmission. The receiver has two methods for synchronizing its clock with the transmitter. Either the receiver looks at the falling edge of the initial start bit of a transmission to synchronize and thereafter reads in the center of all expected bits, for example if each data bit lasts for 16 clock cycles, a data bit is sampled at the 8th clock cycle [33]. The other method for synchronization is that the receiver resynchronizes after each change of the data line, this method is preferred since it handles small diversions from the expected baud rate better. Both synchronization methods described requires that the baud rate is defined with both the transmitter and the receiver.

4.6 Operational Amplifier

An operational amplifier, from now referred to as an op amp, is a device that amplifies a signal. It is designed to be used with external components in a feedback loop. The feedback components and feedback loop design determines the function or operation of the amplifier which can perform different operations and thereby its name. Different operations could be to add, subtract, average, integrate and differentiate. [34]

An op amp usually has 3 terminals except the ones dedicated to power supply; inverting input marked with a minus sign, non-inverting input marked with a plus sign and the output. The inputs ideally have infinite impedance and the output has zero impedance. The op amp amplifies the difference between the input terminals, if both terminals has the same potential ideally the output should be 0. An op amps gain can be of 4 different types: voltage to voltage (voltage amplifier), current to current(current amplifier), voltage to current (transconductance amplifier) and current to voltage (transresistance amplifier). In this case only the voltage amplifier is of interest.

The voltage amplifier can be configured in 2 ways, either with the output out of phase with the input which is called inverting configuration (Figure 11) or with the output in phase with the input which is called non-inverting configuration (Figure 12). Both types utilizes a negative feedback loop, where the ratio between feedback resistor and input resistor determines the gain of the amplifier.

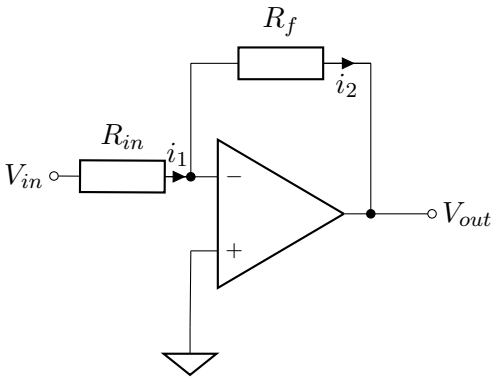

Figure 11: *Inverting op amp*

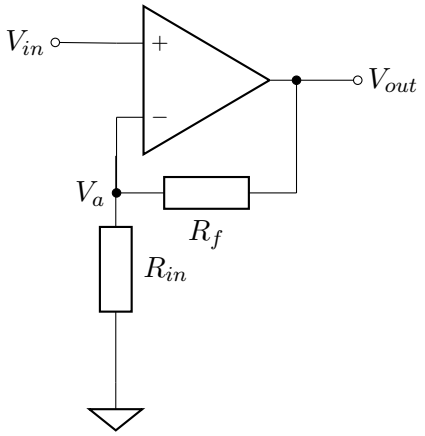

Figure 12: *Non-inverting op amp*

The output of the op amps drives the inverting input via the feedback loop to the same voltage as the non-inverting input. Therefore in both configurations the assumption is made that there is no voltage difference between the inputs of the op amps.

For the inverting case this means that there exists a "virtual ground" at

the inverting input. Then it is possible to determine by Ohms law $i_1 = \frac{V_{in}}{R_{in}}$. Since the inputs to the op amp ideally have infinite impedance, no current can take that way but has to go through the feedback loop, this means that $i_1 = i_2$ and that the output voltage can be described as $V_{out} = i_1 \times R_f$. Combining the 2 equations, having in mind that it is an inverting amplifier and solving for the gain which is the output voltage divided by the input voltage yields Equation 7.

$$\frac{V_{out}}{V_{in}} = A = -\frac{R_f}{R_{in}} \tag{7}$$

In the non-inverting configuration, the same assumption is made and therefor $V_{in} = V_a$. The resistances can be seen as voltage dividers from the output and therefore $V_a = \frac{R_{in}}{R_{in}+R_f} \times V_{out}$. Combining these 2 equations and simplifying yields the ideal gain for a non-inverting amplifier according to Equation 8. [27, chapter 2]

$$\frac{V_{out}}{V_{in}} = A = 1 + \frac{R_f}{R_{in}} \tag{8}$$

4.7 The Doppler Effect

The Doppler Effect was first described by Christian Doppler in 1842. It is the phenomena that describes the frequency change of a signal that can be heard from example a sound source that is moving. A typical example is when an ambulance or police car is driving with the sirens on. First when the car is moving towards you, you will hear a higher pitch in the sound and when the car is moving away a lower pitch will be heard. This phenomenon can be described as when the emitting object is moving towards the observer, sound waves will be detected faster and thereby the perceived frequency for the observer will be increased. The other way around when the emitting object is moving away from the observer, the time it takes for each sound wave to reach the observer will be extended, and thereby the observer will experience a lower frequency.

The Doppler Effect can be seen in different media and in different sources, as in acoustics, light and other electromagnetic waves. The frequency shift in light causes the light to change color and is widely used in astronomy to calculate which speed stars and galaxies are moving towards or away from us. The Doppler Effect also occurs when the sound wave reflects of a moving object. This can be used with ultrasound to detect speed and flows of different materials. [12, chapter 15-5]

5 Ultrasonic Positioning System

5.1 System Overview

The ultrasonic measurement system consists of two main parts; the slave modules and the master module. The slave modules are responsible for providing measurement of the distance to the ground from the point it is located. The slaves are mounted in an array with a fixed and known distance between each sensor. The same sort of microcontroller that is used as master is also integrated in the slave modules. A road dummy with the same dimensions as an actual road section of the ERS has been used throughout the project for measurements which can be seen in Figure 13.

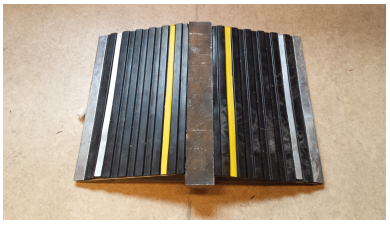

Figure 13: *The dummy of the road part of the ERS*

5.2 Master Module

The master module is responsible for gathering the measurement data from the slaves and compiling it to determine the relative distance for the vehicle, the master module can be considered the central processing unit (CPU) of the system. The master module consists only of a microcontroller connected to the computer via USB and to the I^2C(4.4) bus, where the slaves are connected. The master module is powered via USB and therefor a common ground with the transducer modules is required in addition of the I^2C-wires.

5.3 Slave Modules

The slaves are the measuring devices that sends out a burst of ultrasound (ultrasonic ping) from an ultrasonic transducer and measures the ToF until it detects the reflected echo by using another transducer. An ADC samples the returning echo and measures the ToF. The sampled data is stored directly in the memory of a microcontroller using DMA. An ultrasound ping is transmitted and sampled when the master requests so. The slave module also calculates the distance of where the echo first reflected and transmits the calculated value to the master when the master requests it. A photo of the slave module is displayed in Figure 14

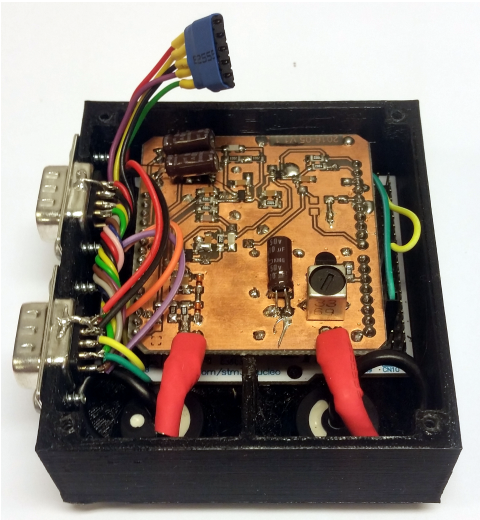

Figure 14: *Slave Module, the printed circuit board mounted on top of the MCU. Transducers are connected in the lower part of the figure*

The slave microcontroller is mounted inside a case. In the case, there are two D-SUB 9 female connectors which allow the slave to be connected to two other modules. The case contains, apart from a microcontroller and two transducers also a header on which there are mainly two different circuits, the ping circuit and the amplifier circuit. The ping circuit transforms the output from the microcontroller to transmit sound of a higher amplitude. The amplifier circuit filters and amplifies the returning signal before the microcontrollers ADC samples it.

5.4 System Setup

The power supply for the master and the slave modules originates from different sources, the master is powered via USB from a computer whereas the slave modules are powered from an external PSU. The master module is connected to the slave modules via I^2C interface and since they are powered from different sources, they also need a common ground.

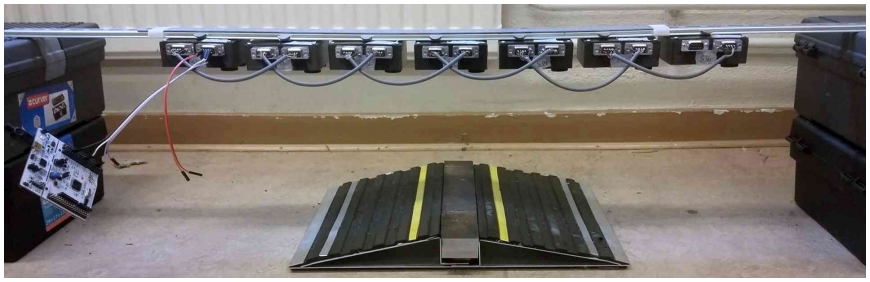

Figure 15: *The setup of the ultrasonic positioning system containing 7 slave modules and the master to the far left in the figure. The unconnected wires in the left part of the figure is for power supply to the slave modules. Ground is connected to the connector on the sides of the slave modules.*

The slaves are evenly positioned on a DIN rail as can be seen in Figure 15. The slave modules of the array are linked together with D-SUB9 male to male wires. The wires are internally connected within each of the slave module to bypass the connection to the next slave. All of the 9 conductors in the wire was connected for future use, even though only 4 is used at present (2 for power supply and 2 for I^2C). The DIN rail placed on top of boxes in both ends to elevate it from the ground, the road dummy for the ERS is placed on various points beneath the DIN rail.

6 Method Summary

This section describes the procedure throughout the project. The project plan for the initial project differs somewhat from the one presented in this report due to complications during the project and also because the complexity of the project became higher than anticipated.

In the beginning of the project, a time plan was implemented in a Gantt chart. The different milestones planned was the larger parts of the project. A long with the time plane, a log book was started and every day during the project, a few comments was to be written in the log book about the procedure of the project and what has been done.

The first part of the project was to read in to the topic by conducting an ultrasound literature study to get a deeper knowledge of ultrasound and to have a foundation stone to start the project from. (The important parts of the study can be found in Section 3).

Initially the code was written on an ATmega88 with the intention to use an AVR as the final CPU. It was soon discovered that the ATmega88 had a too slow clock frequency to provide a 40 kHz PWM signal for the transducers. Therefore, an external timer circuit was implemented to provide the PWM.

Thereafter, an algorithm was written to be able to find the relative position of the ERS elevation after being provided with accurate data. The algorithm was at first stage developed and simulated in computer program, and thereafter a test-rig was built using Arduino ultrasonic distance sensors to validate and see how accurate the algorithm would be with cheap, relatively inaccurate sensors.

A microcontroller that could both sample at sufficient rate and also perform the calculations required relatively fast was needed. It came to our knowledge that the Nucleo-64 development board met the requirements, it could also provide a 40 kHz PWM signal directly from an output-pin. This MCU was ordered and evaluated, the code used in the final design was programmed in stages and evaluated after every added stage. At first a breadboard solution was implemented, apart from smaller implementations, most of the setup was pre-built. During this setup, the code to find the distance between the transducer and the reflecting surface was developed. The amplification of the returning signal was investigated, to find a solution that provided a good signal for the ADC. Also the circuit to trig the emitting transducer was settled in order to provide as high amplitude of the emitted sound as possible.

The next goal was to build a PCB as a shield to mount on top of the MCU. The shield holds the amplifying circuit and the ping circuit from the breadboard. A first prototype of PCBs was designed and components were ordered to produce the circuit boards in-house. After the first prototype had been tested and revised, an improved second prototype was designed

and new components were ordered. The second prototype was also the final version of the circuit board in the project.

The final part of the project was to mount all of the transducers in an array and evaluate their accuracy and repeatability for distance measurement. The purpose was also to compile the distance sensors measurement data to determine the position ERS elevation. The remaining time of the project was spent on testing the ultrasonic positioning system and to develop the software for the MCUs further, and also to administratively compile the results.

7 Implementation

7.1 Simulation and Modeling

7.1.1 Correlation Method

The correlation method is a relatively complicated algorithm. The basic idea is to compare the returning ultrasonic echo with an ideal predefined shape of the echo. When the echo has returned, it is compared with the ideal signal by cross correlating(Section 4.2) the two, when the highest value of the correlation is detected, the best match has been found and a guess of when the echo started to return can be determined. To get a good display of the returning echo it is important to have a high sample rate.

The sampling rate needs to be relatively high, since this is determining the resolution of the result. The result is being fitted with that accuracy. For example, if the sampling rate is 1 MHz, the resolution of the returning signal will be one sample each 0.34 mm according to Equation 9.

$$d = \frac{v}{samples/s} \tag{9}$$

Where d is distance and v is the velocity of sound in air and is approximated to 340 m/s.

7.1.2 Detection of Road Algorithm

To determine the relative distance to the ERS elevation on the road, a sort of convolution is used. Since the shape of the ERS elevation is known, this information is used along with the calculated distance from each ultrasonic sensor module to the reflecting surface underneath.

Each of the ultrasonic sensor modules provides a distance, since the ERS elevation is 41 cm wide and the sensors are spread over a span of 60 cm all sensors will never send an ultrasonic ping against it simultaneous. The distance to ground therefor assumed to be at the level of sensor providing the highest distance.

A model has been built up of the ERS elevations shape to be used in the algorithm. This model is built up with 42 values saved in an array, one value at each centimeter of the elevations 41 cm width. The values are the elevation from ground in millimeters, ranging between 10-50 mm.

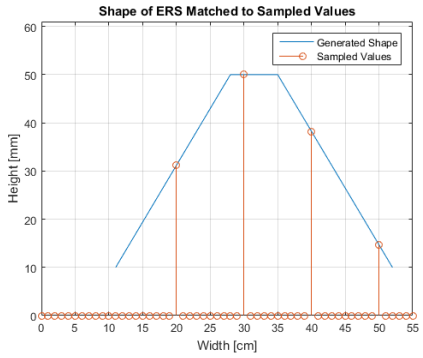

Figure 16: *The generated shape of the ERS elevation is adjusted to where the match is best. The distance where the generated shape starts represent the distance in cm on the first sensor in the array of ultrasonic sensors. Sensors are mounted every 10 cm.*

In this case correlation and convolution are the same thing, due to the symmetry of the ERS. The shape is compared to the calculated data by performing a variant of convolution, what differs this algorithm from a regular convolution is that instead of multiply every element, the absolute value of the difference of the elements is used. This convolution will therefor not yield in a peak where the arrays matches as best, instead the best guess of where the ERS elevation is located is defined as a low point between two peaks. Since the values from each slave module is known, the search for the low point is made around the slave module that provided the lowest value and thereby the highest detectable elevation from ground. This method is preferred to a conventional convolution for the reason that a convolution would give the highest peak where the product of the elements in the array is as large as possible and not necessary where the shape of the stored ERS elevation matches best with the measured data. The differential convolution will ideally however, always give a low point where the shape matches best. In Figure 16 is an example of ideal distance measurement values and in Figure 17 is the calculated relative distance presented where the results between the differential convolution and convolution differs.

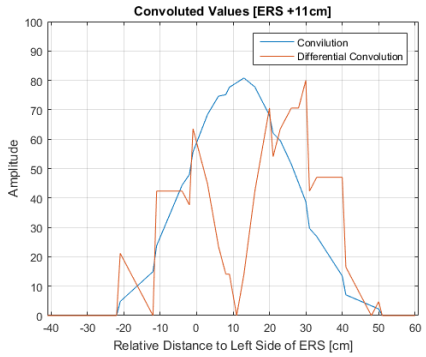

Figure 17: *Shows the difference between the convoluted value and the differential convolution used in this project. The differential convolution has its lowest point at the distance on the array of ultrasonic sensors 11 cm. The convoluted value gives the highest point at 13 cm.*

The convoluted value will always give a value close to the actual, therefor it might be interesting to look for the lowest point on the differential convoluted array around the highest value of the convoluted array. Since the arrays are of same length, the index of the highest value in the convoluted values can be roughly translated to the lowest point of the differential convoluted array. This is assuming that the processors calculation time is not a limiting factor.

When the distances are calculated by the slave modules and provided to the algorithm, they are put into another array, divided into 61 values, each value represents a centimeter.

The algorithm developed for determining the relative distance to the elevated road is dependent of accurate measurement values from all of the sensors.

7.1.3 Determine Distance to Ground Algorithm

The algorithm uses the raw data sampled by the slave modules via Direct Memory Access (DMA). The microcontroller uses this data to correlate with an ideal predefined echo. The ideal echo has been sampled using the same module.

The ideal echo values are defined from measuring an ultrasonic echo which reflects of a point source. As the point source, in this project a thin pencil was used. The idea behind using a point source to compare with instead of a flat surface, like the one more probable to be found under a vehicle, is that the reflected signal from any given point on a flat surface would be identical to the one reflected from a point source. Since there are multiple points on the surface the result of the echo from the flat surface will be comparable to a signal reflected from a point source. Since the surfaces

that will be targeted are not always flat and perpendicular with the emitted sound wave, for example the electric roads elevation is tilted and asphalt has a rough surface an echo from a point source is sensible to use as a comparator.

The correlation is performed by using FFT of both the sampled data and the ideal data. As a multiplication in the frequency domain is equivalent to a cross-correlation in the time domain. Using fast Fourier transform is a considerably faster method than using correlation in the time domain. See Section 4.2.

After the data are transformed to frequency domain, the sampled data are complex conjugated and thereafter multiplied element by element with the ideal pre sampled echo. Thereafter the data are transformed back to time domain using the IFFT as shown in equation 5 where x is the sampled data and y the ideal echo. Since correlation using FFT wraps around the resulting array, it needs to be shifted in the correct order to be equivalent to a time domain cross-correlation. The shift has been handled by the algorithm to put the data in the correct order. This simplifies the analysis of the data during development. The best calculated fit of the cross-correlation occurs on the position in the array where the largest element is. This means that the sampled data matches the predefined echo as good as possible. And the position in the array can be translated to a distance according to equation 9 since the data is shifted in the correct order.

When the peak of the cross-correlated value has been detected, the value of the peak in the array represents the number of sample the ADC has converted since the sampling was initiated.

it is possible to backtrack to where the echo started to be recorded since it is known where the ideal echo started. The time is known since the ADC is started immediately after the ping is sent. Assuming no lag occurs between the different slave modules that would delay the ping. This distance in samples can, if preferred, be translated to a distance in millimeters, but has not been used in this project. Instead the number of samples until the echo has been detected is used as distance measurement.

The analog to digital conversion is started directly after the transmitting transducer is trigged. This means that the first sample of the sampled values has a minimal delay to when the transmitted signal has been conducted. It is the relative distance for all sensors at every given moment that is of interest. The sound propagation in air is therefore assumed to be constant even though it is dependent on air temperature.

The ideal pre-sampled echo is initialized in an array that allocates spaces for 4096 floating points, it is Fourier transformed during start-up of the microcontroller and thereafter stored. The array that handles the ADC sample values stores 1024 values in 8 bit resolution. This array is only temporary and is the array where the DMA stores the converted values. These values are after every ultrasound ping transferred to an array containing 4096

floats and thereafter fast Fourier transformed. The FFT algorithm stores the real and imaginary values alternatively in the arrays. These are thereafter multiplied element by element where the real value and the corresponding imaginary values fetches from the arrays. The complex multiplication is performed according to equation 10.

$$X \circ \overline{Y} = (a_x + ib_x) * (a_y - ib_y) \tag{10}$$

This equation shows a multiplication of the two complex values X and Y where the latter is complex conjugated. a is the real and b is the imaginary part of each value.

7.2 Test of Detection of Road Algorithm

To test and evaluate how the simulated algorithm works on a physical system a small scale test rig was built. This was also a keystone to see the limitations of the system and a good rig to test different scenarios and width between the sensors on the array. To get a visual feedback of the algorithm, a cable railway with pulleys were built. The cable is driven by a the stepper motor. A metal piece is hanging from the cable to imitate the pick-up. When the MCU has calculated where the ERS road dummy is located, the MCU tells the motor to take as many steps as needed for the metal piece to move to that position.

7.2.1 Arduino Mega 2560

Arduino was chosen as MCU. This because of its simplicity and it enables rapid development with built in libraries for software and a lot of different gear and accessories for hardware. The Arduino Mega 2560 board uses the 16 MHz Atmega2560 microcontroller from Atmel, see Figure 18. The MCU has sufficient amount of digital input outputs for this application. Several of the I/Os can be used as independent PWM signals. A communication with Matlab via USB is establish to enable analysis of the measurement data in the computer. The power supply to the MCU comes from the computers USB-port. [35]

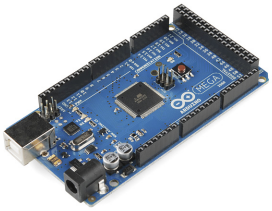

Figure 18: *Arduino Mega 2560 development board. [36]*

7.2.2 HC-SR04 Distance Sensor

The HC-SR04 distance sensor utilizes 40 kHz ultrasound to measure the distance to objects in front of it, which is shown in Figure 19. It uses one transducer as a transmitter and another as receiver and can measure distances from 2 cm up to 4 m with an accuracy of +/-3 mm and a spread angle of 15°. In this application, the sensors are supplied with 5 V directly from the MCU. This sensor uses a threshold detection(Section 4.1) of the receiving echo. The rig consists of seven sensors evenly distributed over 60 cm, which gives a distance of 10 cm between each sensor. [37]

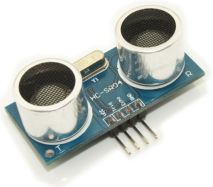

Figure 19: *HC-SR04 ultrasonic distance sensor. [38]*

7.2.3 Stepper Motor

A Phillips stepper motor with a step angle of 7.5° was used to drive a timing belt to get visual feedback. The stepper motor is connected to the LM298 dual H-bridge module described in section 7.2.4. The stepper motor has four windings, they can either be wired two by two in series or parallel connection. Depending on how the windings are connected different torque and power settings will be achieved. The axis of the stepper motor is connected to a 2.54 mm (1 inch) pulley. The smallest distance the stepper can move the pulley can be calculated in Equation 11. In this case the smallest distance is 0.4 mm.

$$\frac{distance}{step} = d\pi \frac{\theta_{step}}{2\pi} \tag{11}$$

Where distance for each step of the stepper motor is given. d is diameter of the pulley, θ_{step} is the step angle in radians.

7.2.4 H-bridge Motor Driver

To be able to control the stepper motor a LM298 dual H-bridge module was used, see Figure 20. The H-bridges are connected between the motor and the MCU. Four wires are connected between the MCU and the H-bridges, two of the wires are used to enable the different H-bridges and the other two are used to transfer a PWM signal. On the motor side of the H-bridges, the two windings are connected to each of the H-bridges. The H-bridge module is powered from a 24 V external PSU. A common ground is connected between the Arduino and the H-bridge module.

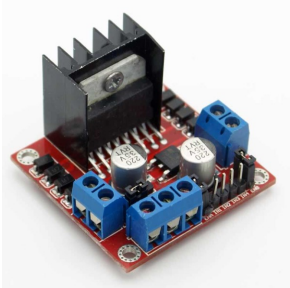

Figure 20: *LM298 Dual H-bridge module. [39]*

7.2.5 Implementation of Test Rig

First one sensor was connected to the Arduino to test and see how it works. To measure the distance an open source library called Ping was downloaded and used with the Arduino Mega. The library has support for multiple sensors and the next step was to try and connect them all and measure the distance from each sensor. When all sensors worked with the Arduino Mega the simulated road finding algorithm needed to be implemented into the MCU.

A wooden plank became the base of the rig. First the sensors were glued to one side of the plank with a distance of initially 15 cm between each sensor, but the distances were later decreased to 10 cm. Long cables for power supply and communication with each sensor were also glued along the plank and connected to the Arduino Mega. The wooden plank was then placed about 20 cm above ground with the sensors aimed downward. To ensure that the plank was in level a spirit-tool was used. The road dummy was placed underneath the sensors and various positions were tested

to simulate the vehicles different relative positions due to lateral movement. The Arduino rig with cable railway can be seen in Figure 21.

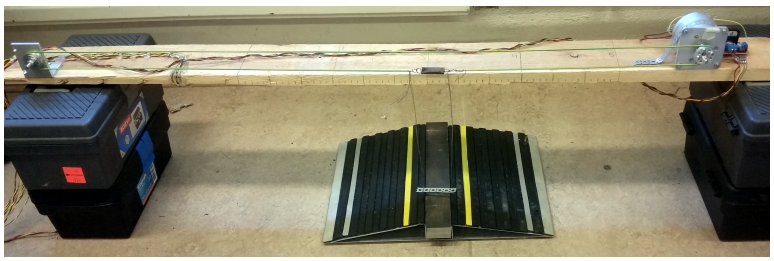

Figure 21: *Cable railway to simulate ERS pick-up. Ultrasonic sensors are mounted on the underside of the wooden plank.*

In order for the road finding algorithm, described in Section 7.1.2, to work properly, it was first tested to measure the distance of each sensor to the ground and to see through that they all gave a similar result. Next step was to place the road dummy beneath the sensors and make a new measurement to see how accurately the MCU could position the road dummy relatively the position of the sensor furthest out on the array.

In an attempt to increase the resolution of the measured values and to avoid the sensors to detect the second and third reflection, a median filter was implemented where a number of measurements were performed from each sensor. All the values received from each sensor was sorted and the median value was chosen.

After the distance between each sensor was decreased from the initial 15 cm down to 10 cm interval, more tests where done to see if the systems performance were good enough and if there were any improvements.

7.3 Laboratory Equipment

- DC regulated power supply (ATTEN TPR3003T-3C Triple channel)
- Soldering stations
- Function Generator (FG1201B)
- 3D printer (Delta Rostock mini G2s)
- Multimeter (BS3604W BST)
- Oscilloscope (Rigol DS1054Z)

7.4 Choice of Transducers

To get the best possible transducer for the application that fits the projects requirement, a small investigation of different transducers were made. The

broadband electrostatic transducers were considered too expensive for the project and not feasible for a future commercial application electrostatic transducers are also unsealed which makes them unfit for outside use. Therefore, focus was on the cheaper narrowbanded piezoelectric transducers. In the lab two different piezoelectric transducers were found, as shown in Figure 22. One of them was a transducer with open membrane, which has the advantage of good sensitivity, but the disadvantage that it is not waterproof. The other transducer was sealed and therefore waterproof but has lower sensitivity instead. When searching for other piezoelectric transducers on the internet, mainly these two types of piezoelectric transducer were found. After some investigation, it came to our knowledge that parking assistance sensors for cars are in fact piezoelectric transducers which are sealed and made for the type of environment that is on the outside of a vehicle. Therefore, a quick search on three scrapyards were done, but with no luck. Most of the cars were too old to have parking sensors, and on the newer ones the complete rear bumper with sensors was sold as a spare part and exceeded the budget.

After this it was discovered that Biltema warehouse retailed retrofit parking assistance kits which included four ultrasonic piezoelectric transducers in each kit. Initially one kit was bought and the sensors were tested. After verification that the transducers fulfilled the projects requirements, three more kits were bought providing a total of 16 sensors. The three different sensors that were tested can be seen in Figure 22.

Figure 22: *The three different transducers that were tested in the project all of piezoelectric type. From left to right: Unsealed transducer from lab, sealed transducer from lab and Biltema transducer*

7.5 STM32F303RET6 Microcontroller

7.5.1 Specifications

The microcontroller used in the project was the STM32F303RET6 Nucleo board, see Figure 23. The microcontroller is produced by STMicroelectronics. It is a development board which provides an on board field programmer that connects to a computer via USB. It is possible to communicate with

the microcontroller in real time over USB via the UART/USART hardware.

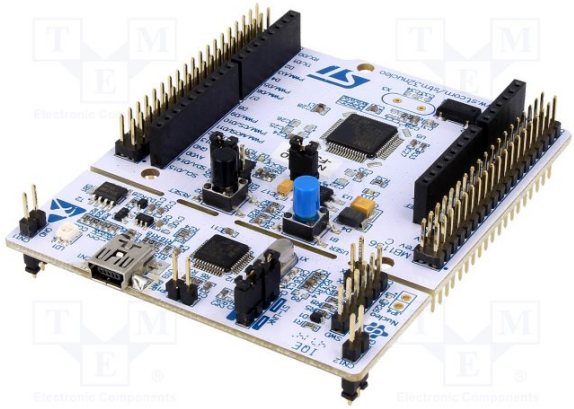

Figure 23: *Nucleo-64 Development Board, Model;STM32F303RET6. [40]*

The architecture is built up on a 32 bit ARM cortex processor. The processor has a clock frequency of 72 MHz. The processor also has hardware support for FPU which allows fast operations with floating point units. The controller also contains 80 kB of RAM.

The controller holds 4 different ADCs, of those, two has DMA. If the two DMA ADCs are combined it is possible to sample at over 10 Msps with 12 bit resolution. In this project only one channel is used and the resolution is 8 bit, if no prescaler is used, the single channel samples at over 7 Msps second at 8 bit resolution. [41]

The controller also come equipped with 4 integrated op amps.

For communication, the controller leaves several options. It has I^2C, UART, USART, SPI, USB and CAN.

7.5.2 Modification of Microcontroller

Some hardware modifications have been made on the microcontrollers that are used in the slave modules. The most conspicuous modification is that the part for programming and connecting to the computer has been removed. The programming device can still be used to program the microcontroller if pins are connected to the microcontroller from the programming part. The microcontroller also need external power supply when it is being programmed and when it is being used since it no longer can be powered from an USB port. To ease the access of the programming pins of the microcontroller an in-house manufactured connector was soldered onto the pins used for programming on the microcontroller. The pins connected was Vdd at the microcontroller, clock, ground, data input/output and reset. The wires that were attached to the connector were covered with shrinking hose in

the splice points to not risk any unexpected short circuit between the wires. (see Figure 24)

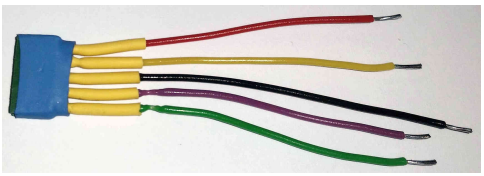

Figure 24: *Connector for programming and debugging the microcontroller*

Another permanent modification that was made on the microcontrollers were to cut off all the pins of its underside. All of the pins are still represented on the top of the microcontroller and the modification does not affect the functionality in any way. By cutting of the pins, 6-7 mm of the microcontroller height could be removed. The pins are visible under the MCU in Figure 23.

The last hardware modification was to solder on an external 8 MHz oscillator crystal on all of the microcontrollers used. This was the only hardware modification made on the master module. Before it was possible to use the extern crystal, it needed to be connected to capacitors connected to ground on both pins, also jumpers needed to be soldered on to connect both pins to the CPU. The components are listed in the bill of material in Appendix A.

7.5.3 Configuration of Peripherals in Stm32CubeMX

There are several configurations made in STM32CubeMX, this applies for all the peripherals that are used on the microcontroller. There are different configurations on the transducer modules and the master module.

In the master module configurations have been made on one I^2C channel and one USART channel and the register Reset and Clock Control (RCC).

In the slave module, configurations have been made on one ADC channel. two Timers, two I^2C channels, DMA and RCC.

The ADC was configured at a sample rate of 225 kHz in 8 bit resolution with DMA. The timers were used to set a PWM output which was used to initiate the ultrasonic ping. The two timers control the PWM signal and the duration of the PWM signal. The PWM signal had a duty cycle of 50 % when a ping was conducted and 0 % when idling.

The 8 MHz crystal was scaled up to 72 MHz which is the standard frequency of the microcontroller. The I^2C channels was set to 100 kHz mode both for the on-board communication of the slaves with the digital potentiometer and with the bus communication between the modules. The UART communication between the master module and the computer was set to a baudrate of 115.2 kbits per second.

To see specific configurations of the controller in the different modules see Appendix B.

7.6 Prototypes for Ultrasonic Sensor Modules

7.6.1 Development Environment for Hardware Design

During the build of the sensor modules, different development environments were used. For the circuit design and board layout of the PCB shield, EAGLE 7.2.0 CAD software was used.

To simulate the circuit design and see if the design works before etching of the PCBs LT Spice IV was used. LT Spice is a simulation software for electronic circuits developed by Linear Technology. LT spice allows circuit designs to be tested to see if it works as intended.

The cases for the sensor modules was designed in SketchUp. SketchUp is a free CAD software which is easy to use and good for simple designs. It was chosen because of previous experience.

The 3D printer uses a program called Repetier Host which is used to control the printer. Repetier also utilizes another program called Sli3er, which is the program that converts the 3D model to instructions for the printer. The printer can either use PLA or ABS plastic. ABS requires a higher printing temperature than PLA, whereas PLA is more fragile when in solid state than ABS. ABS shrinks more when it solidifies compared to PLA which increases the chance that it misshapes. PLA was chosen because it was already mounted on the printer.

7.6.2 Development on Breadboard

The first setup utilized a prebuilt amplifier circuit board designed for ultrasonic transducers that are used in the course *Industrial Measurement Systems for Control* given by IEA at LTH. This board together with an oscilloscope and a prebuilt ping circuit also from the same course was used to test the different transducers described in Section 7.4.

The amplifier circuit board consists of two operational amplifiers, first one configured as an non-inverting amplifier and a second op amp configured as a inverting amplifier. Both amplifier stages utilize filters in their feedback loops to get rid of disorders and noise. On the input to the first amplifier there is a first order low pass RC-filter which suppresses the high frequencies. The filters cut-off frequency is placed high enough to not suppress the 40 kHz signal from the transducer. To protect the operational amplifiers from voltage spikes a clamper circuit with diodes is utilized in the input stage where one diode connects to ground and one to Vdd. The LM318M operational amplifiers are used which are of dual rail type and therefore needs both positive and negative supply voltage. The amplifier board is connected to a power supply with +/- 18 V. The first amplifier stage has

a fixed gain of 100 and the second stage has a variable gain between 10-30, this means that the combined stages gain can be varied between 1000 and 3000.

The ping circuit was the first crucial part that needed to be done. After some development a schematic with the 555 timer circuit and a push-pull amplifier stage was built on a breadboard. The 555 timer was configured in a stable mode with oscillations of 40 kHz to match the transducers. This circuit worked fine but needed a supply voltage around +/- 15 V to work. This circuit was built because the first MCU that was used, the AVR ATmega88, were not able to generate a PWM frequency of 40 kHz. This circuit was also used to test the transducers in company with the same amplifier board.

The microcontroller that was later chosen for the project was able to generate a 40 kHz PWM signal, therefore there was no need for the 555 timer circuit anymore. To get an idea of a possible ping circuit for the sensor module, the parking assistance kit circuit board was reversed engineered. This circuit board revealed that they used a switching transistor connected to the primary side of a transformer. The secondary side of the transformer was connected to the transducer. With a voltage supply of 8 V to the primary side of the transformer this yielded a voltage of 80 V to the transducer. This implies that the transformers relationship between primary and secondary side is 1:10. After scanning the market, comparable transformers was found. An order on two different suitable transformers was placed to evaluate them. The transformers internal inductance were 10.6 mH and 6 mH. The transformers inductive qualities form a resonance circuit with the transducers capacitive properties. Therefore, the transformers secondary side needs to be matched with the transducer, to get the right resonance frequency. Figure 25 shows the design of the ping circuit used.

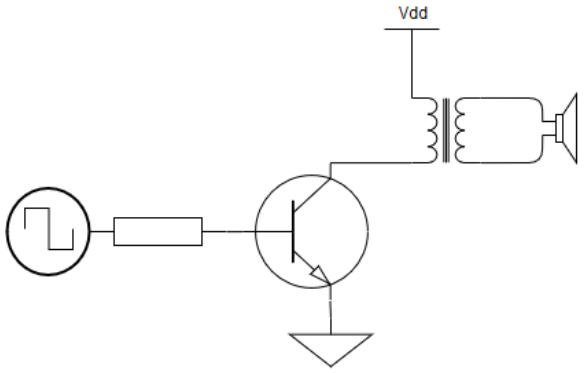

Figure 25: *The ping circuit used. The square wave is generated by the PWM output of the MCU. It has a frequency of 40 kHz and 50 % duty cycle.*

The microcontrollers ADC samples voltages in the interval 0-3.6 V. But

the prebuilt amplifier has an adjustable gain between 1000-3000 and with an amplitude of 5 mV from the transducer signal as input to the amplifier this yields an output of +/-5-15 V oscillating around 0 V. Therefor a bias circuit was needed to be able to connect the amplifier board to the microcontroller. The input of the bias circuit was a voltage divider with resistances that gave one tenth of the signal, so the amplitude was reduced to a maximum of 1.5 V. After the voltage divider a capacitor was used to only let the AC signal through and to block the DC from the bias. A bias of 1.6 V was added over a resistor to the signal, which means that the signal swing to the ADC was 1.6 V +/- 1.5 V.

A number of different tests were performed with this breadboard solution. This setup was used to evaluate the different materials and their capabilities to suppress ultrasonic cross-talk between the transducers. The materials tested was aluminium, plastic, rubber, wood and cork. The measurements were sampled in the oscilloscope and exported to Matlab via a USB memory and analysed. This last setup on breadboard, with the transformer ping circuit, bias circuit and prebuilt amplifier became the foundation for the first prototype shield for the microcontroller.

7.7 Printed Circuit Board Etching Process

To manufacture a double sided Printed Circuit Board (PCB) by etching, the designed circuit needs to be printed on two transparent overhead papers, one paper for each layer. The overhead paper is thereafter aligned on each side of a double sided copper laminate with the printed side of the overhead paper facing the copper to allow less Ultra Violet (UV) light pass between the overhead paper and the copper laminate.

The copper laminate is coated with a positive photoresist that when exposed to UV light weakens the coating on the exposed area, allowing the copper under the coating to be removed by etching. The copper laminate is put inside a cabinet which illuminates the copper laminate and removes the photoresist that is not covered by print on the overhead papers, this process transfers the lithography of the designed board layout onto the copper laminate. The copper laminate is exposed for UV light until all unwanted photoresist has been sufficiently weakened to be removed by the developer. After the illumination the print needs to be developed in a development tank. The development tank contains sodium hydroxide ($NaOH$) which is a basic fluid that develops the coating of the copper laminate not illuminated by the UV light and removes the illuminated areas.

The copper laminate is thereafter submerged in the etch tank. This tank is filled with sodium persulfate ($Na_2S_2O_8$) diluted with water which results in an acid. The tank keeps the temperature at around 50 °C and keeps the fluid in motion with air bubbles in order to speed up the etching process and get an even result. After the etching is completed, all unwanted copper

is removed, the rest of the photoresist should be removed as well. This is done by either illuminate the copper laminate again and lower the copper laminate in the development fluid, or by cleaning the photoresist off by using an alcohol.

All vias and hole-mounted components needs drilled holes. This is done by using a small drill, and a high precision drilling machine.

7.7.1 First Prototype

Based on the breadboard solution, a PCB was developed for the shield. Some components from the breadboard solution was replaced. Since the Nucleo development board only can provide a single rail supply of either 5 V or 3.3 V, the operational amplifiers were replaced with low voltage single rail supply amplifiers this was to neglect the need for an additional external PSU. The op amps are powered from the 5 V line. The change of operational amplifiers yielded more changes; the bias circuit could no longer be placed after the amplifiers for the ADC, since also the operational amplifiers needed a bias voltage to not lose the negative swing of the signal. The design from the existing amplifier board was the basis for the new amplifier part of the shield, but had to be slightly redesigned. The combined gain of the circuit was also revised, it was decreased from a gain of 1,000-3,000 down to a maximum of 600. The bias is held by a voltage reference IC, which delivers a reference of 1.65 V and 3.3 V with high accuracy. The 1.65 V reference is biasing the op amps whereas the 3.3 V is connected to an ADC-channel of the MCU. A DC blocking capacitor is placed on the input of the first op amp, to guarantee that no DC can be amplified.

The gain of the returned signal is adjustable due to an added 10 kΩ digital potentiometer placed between the amplifiers. The output signal from the first op amp is connected to the high pin of the potentiometer. The potentiometer's low side connects to ground and its wiper is connected to the second op amp. By varying the wiper of the internal resistance a voltage divider is attained that works as a volume control and can lower the amplitude of the returning signal. The potentiometer wiper's position is controlled by the MCU via I^2C communication, the potentiometer needed to be connected to a separate I^2C-channel from the one combining the slave modules in a serial bus system. Since all of the potentiometers has the same 7 bit I^2C address, they would not be able to be controlled individually if they were connected to the same bus system. The idea behind this volume control is to have a larger installed gain on the circuit board and scale down the signal before the second amplifier not to amplify over the rail of the amplifier if the returned signal is of high amplitude. If it has a low amplitude, no scaling should be performed.

When the circuit design was finished for the shield, it was simulated in LT Spice. This was done to ensure that the circuit worked as intended

before investing a lot of time on etching and soldering the PCBs. When the simulation of the circuit looked promising, the PCB layout was designed. To get more space and to make the routing of the traces easier, a double sided PCB was chosen. On the top layer most of the signal traces was routed and the bottom layer was used primarily as ground plane. The supply lines were also routed in the bottom layer. Several of the electrical components used in the layout was designed in the project to make sure that their solder pads matched the recommendations in the components datasheets. The traces width was chosen to 16 mil and drill holes with 1.1 mm in diameter. When the board layout was finished, two prototypes of the shield was built in-house. The shields were equipped with loops, used for measurements with oscilloscope to ease debugging of the circuit.

After the etching process and drilling described in Section 7.7 was completed, all of the electrical components, pins and vias was soldered on to the PCBs. At first, the prototypes did not work as intended, this was proven to be because of the high speed op amp used has large bias currents and offset currents due to unbalanced inputs of the op amp. Unbalanced inputs are usually not a problem when the bias and offset currents are small, but in this case it caused the amplifiers to hit the rails on the output. After balancing the inputs of the amplifiers, the prototype shield worked as intended, but total gain was limited to 600 otherwise the impact of the currents was too large.

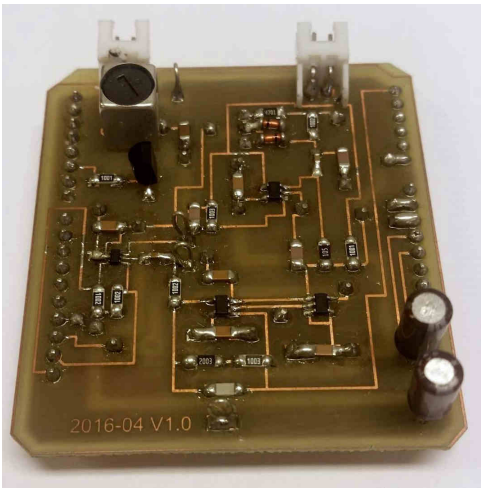

Figure 26: *The first prototype of the in-house manufactured shield.*

There were also problems with electromagnetic interference from the transmitting side to the receiving side. When the transmitting transducer pinged, a cross-talk was detected in the data, which maximized the ADC. To reduce this, a piece of aluminium was inserted between receiving and transmitting side which was then connected to ground.

To be able to make some tests the shield with microcontroller and transducers was attached to an aluminum plate, which in turn was attached to a wooden stick of 50 cm length. See Figure 27.

y 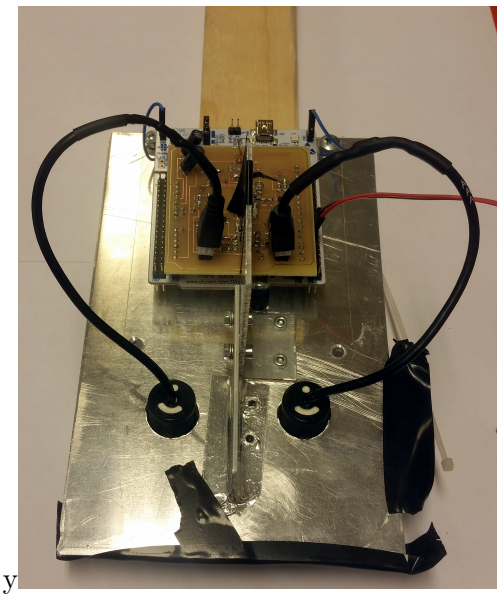

Figure 27: *The first PCB prototype that was used, mounted on a roughly 50 cm long stick.*

Several tests were conducted on this prototype, of which the most important test was to see if the ultrasound echo from the transmitter still could be detected on the receiving side when measured from a moving vehicle. A couple of tests were conducted when driving in different speeds when the prototype was held outside the window of a car with the transducers aimed at the ground. The distance from the transducers membrane to the ground was approximately 1 m.

The transducers were placed in line with the direction of travel with the transmitter first and the receiver 7 cm behind. To see the impact from the wind on the measurements and to try and divert it, different shaped windbreaks was attached in front of the transducers. The different shapes that was tested were a plough and a V-shaped wall see Figure 28 and Figure 29 respectively.

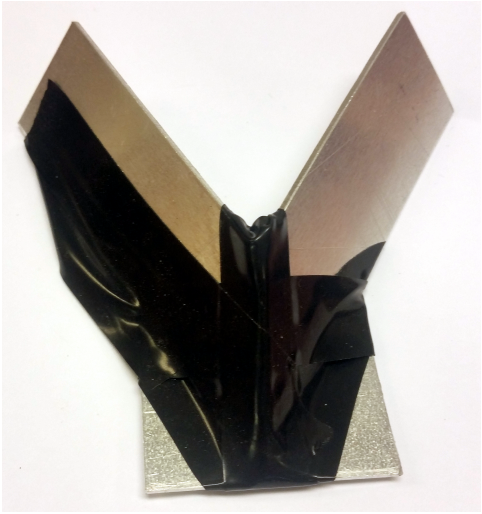

Figure 28: *Plough that was used as windbreak during field testing.*

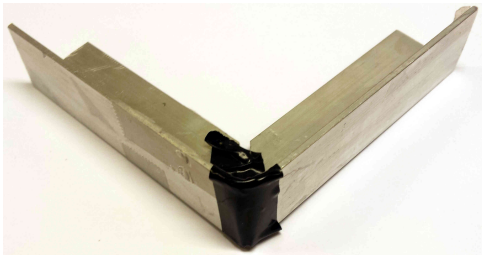

Figure 29: *V-shaped wall that was used as windbreak during field testing.*

The tests purpose is to see if the measurement of the returning echo is distorted due to the Doppler effect or in any other way misshaped and if the echo is detectable with the available algorithms when a vehicle travels at the highest velocities allowed in Sweden. The relative velocity of the wind was not measured during this test.

The tests were performed on the Swedish highway E22, on the section stretching between Lund and Hurva for tests when the vehicle traveled at high velocity (i.e. velocities above 90 kmph). Country road 102 between Lund and Dalby was used for field testing in lower velocities.

When the tests were performed the op amps were set to amplify the signal 600 times and a sample rate of 1.2 MHz, 12 288 samples were stored. The sampling is initiated directly after the PWM signal that triggers the emitting transducer has started.

7.7.2 Final Prototype

After testing of the first prototype some changes to the shield was done. The high speed op amps were changed due to the high bias/offset currents. The new op amps have bias/offset current in pA-scale as compared to μA-scale that the initial op amp had. This results in a freer choice of resistances in the feedback loops of the op amps without balancing problems and thereby higher amplifications. Another change was to add an extra electrolyte capacitor close to the transformer beside the existing ceramic capacitor to smooth out the voltage drop that occur during an ultrasonic ping. The revised design is showed in Figure 30.

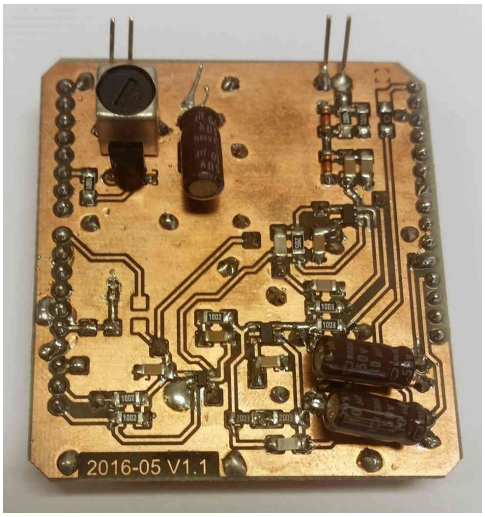

Figure 30: *The final design of the in-house manufactured shield.*

To reduce the impact of the electromagnetic cross-talk from the transmitter side, the distance between the amplifier part and the ping circuit was increased. A second ground plane on the top side of the PCB was also added. A SMD LED was added and connected to a digital pin for debugging purposes. A filter was implemented directly before the ADC input of the MCU, this was however overridden with a jumper and is neglected in the circuit diagram in Figure 31, but the filter is possible to implement in a future application.

Another change from the prototype from Section 7.7.1 is with the clamper diodes, where both of the diodes now connect to ground. One of the diodes connected with anode and one with cathode and vice versa at the signal conductor. This has been done for two good reasons. One is that if one diode was connected to Vdd, the voltage had to exceed the 3.3 V in the power supply by roughly 0.7 V which answers to the forward voltage drop of the diodes, this makes it possible for the input of the first op amp to be set to 0.7 V above its power supply, which could harm the IC. The other reason is practical, to allow the diode to connect to Vdd, a conductor for the power supply would have to be printed there on the PCB which would not be optimal due to EMC so close to the unamplified signal since the cross hearing from the power supply might interfere with the measured signal. This change has no impact on the signal since the signal only has an amplitude in the scale tens of millivolt and the leakage current through the diodes does not seem to affect the measurements.

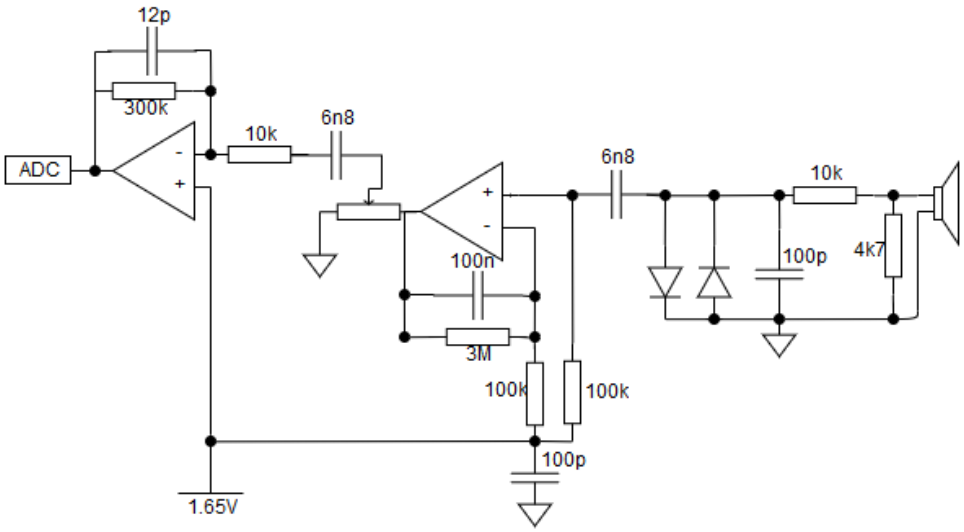

Figure 31: *The circuit diagram of the amplifiers for the ADC circuit. The 1.65 V are provided from a voltage reference circuit and the potentiometer between the op amps is digital and the wipers position can be set from the MCU.*

For the new version of the shield two prototypes was initially manufactured in-house to see if the new design worked properly. After a quick test of the new design and ensuring that they both worked as expected, the manufacturing process for the rest of the shields began and for the complete ultrasound positioning system. The complete circuit diagram with bill of material can be seen in Appendix C.

7.7.3 Building the Ultrasonic Positioning System

A decision was made to build a system consisting of 8 sensor modules. Since two shields already was built, six more was needed. To speed up the manufacturing process of the remaining six shields, all the PCBs was etched and drilled at the same time. With two soldering stations, one for smaller components and one for larger the soldering process could be fairly fast and all in all it took about 2 days to complete all the shields.

Each sensor module of the system needs a housing, after searching for encapsulations at suppliers but not found the right size the decision was made to design and 3D print the housings in-house. A 3D printer was lent from the department of Automatic Control at LTH. First a smaller box was printed to see the results and if the quality was good enough. Then a first prototype for a housing was designed and 3D printed. The dimension of the box was good but some other changes were required, so three iterations was necessary to get an accomplished box see Figure 32. The other parts implemented was holes for D-SUB9 connectors, a partition

between the transducers and changes of the diameter for the transducers holes.

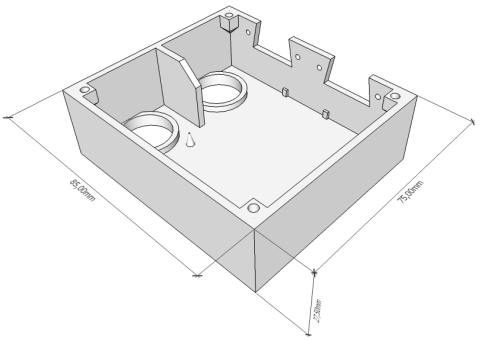

Figure 32: *Rendered figure of the 3D printed box.*

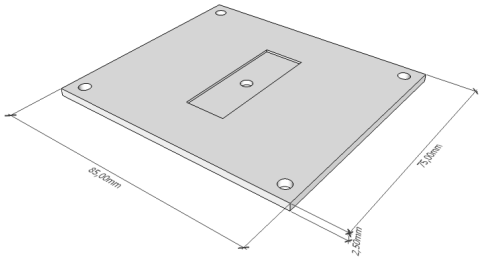

Figure 33: *The lid of the 3D printed case, the submersion in the top is to mount a DIN rail clip for attachment on DIN rail.*

One housing took about 3 hours and 40 minutes for the 3D printer to complete. On average two housings a day was printed, which means that all the boxes took about 4 days to manufacture. An example of a 3D printed box can be seen in Figure 34. In the meantime, software was developed. Also the male D-SUB connectors was soldered together with wires and outlets for the supply and communication.

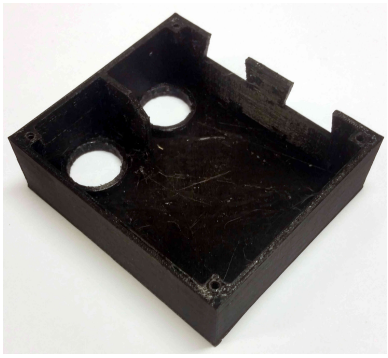

Figure 34: *The printed 3D case for the slave modules.*

The D-SUB wires were manufactured using 17 cm long sections of a 9 conductor wire and solder each of the cables to a D-SUB 9 female connector in both ends. The wire is shielded and the shield is soldered on to the connector in each end. A shrink hose is used to cover the shield of the wire to prevent short circuiting. Figure 35 shows the result. The D-SUB wires are used for power supply and I^2C communication.

Figure 35: *The wire used to connect the slave module with each other and also provide power supply and serial communication with the master.*

The male connectors are soldered together in pairs using 9 different colored wires each roughly 5 cm long. Since the modules are connected in a serial bus, all of the conductors from one D-SUB connector needs to be bypassed to the other. The MCU belonging to every connector is coupled in parallel from the bus. The ground conductor is connected to the D-SUB connector on both ends as can be seen in Figure 36.

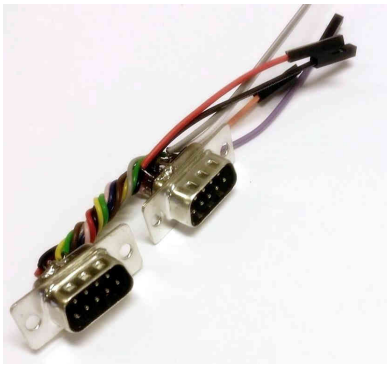

Figure 36: *The connector mounted inside the 3D printed case.*

The structural modifications of the MCUs is performed as described in Section 7.5.2. The programmer of the MCU and the pins were removed in order to keep the size of the housings at a minimum.

Lids of the boxes was also designed and 3D printed, the final design has a submersion in the middle of the lid for a DIN rail clip. The design of the lids is shown in Figure 33. The submersion is there to prevent the boxes from rotating. When all the parts for the boxes was finished the assembly of them could begin. First the connections from the male D-SUB connectors was attached to the development boards, then the in-house manufactured shields were attached to the boards as can be seen in Figure 14. After this, the assembled parts are ready to be put into the housings. The development board is held in place by three spikes in the bottom of the box that matches the screw holes on the MCU board. Then the D-SUB connectors can be screwed to the housing which also prevents the MCU and PCBs from falling

out. Last step was to screw the DIN rail mounting clips to the lids and then attach the lids to the boxes. Now each sensor module can be mounted onto the DIN rail with any suitable distance, but with a minimum width of the boxes length which are 8.5 cm and the maximum width limited by the length of the connector.

7.8 Communication Method

7.8.1 Communication Between Microcontrollers

In order for the MCUs to be able to exchange information with each other, it was necessary to set up a communication system. The communication system used for MCU to MCU communication was an I^2C serial bus described in Section 4.4, which the MCUs have hardware support for. The communication system implemented in a serial bus that only require two wires to connect all MCUs.

Since there are only two wires, with half duplex, only one MCU can send data over the bus at a time. This means that a user defined protocol had to be developed to ensure that conflicts when several units transmits never occur.

When a master contacts a slave it is done with a user implemented high level protocol. The master calls the slave either on its predefined address and transmits a packet or by a general call which is a broadcast that reaches all the slaves connected to the bus. The packet has a size of 4 bytes and contains instructions for the slave of which action that should be performed next. The list of calls and actions can be found in Table 2 where the calls written in capital letters represents macro values defined both in the transducer module and the master module, the number before represent which of the 4 bytes are set to a specific value. When a slave is called, it enters an interrupt subroutine in which the requested action is performed. If the instruction is only to send back the latest measured distance or to change value of the digital potentiometer, it is performed in the subroutine otherwise the task is considered too time demanding to be performed in an interrupt subroutine and therefore the program leaves the subroutine before following the instruction.

Master Call	**Slave Action**
0: BROADCAST 1: Number	If byte 1 is a multiple of the slaves own address, an ultrasonic ping is performed. Else no action is performed.
0: REQ_DISTANCE	Slave transmits the latest calculated distance measurement to the master.
0: SLAVE_PING	The slave performs an ultrasonic ping. And measures the distance to ground
0: REQ_ADC_VALS	The slave return the whole array of ADC samples.
0: SET_DIG_POT 1: Value	The slave sets the potentiometers value to the value provided in byte 1.

Table 2: *The master calls only one slave on its unique address and requests it to take action except if a broadcast is performed, then all slaves are called.*

The slaves enter the interrupt subroutine if the address called matches either the broadcast address or the slaves unique address and if the expected amount of data has been received. It is not known to the slave what type of call have been made. Therefore, the master attaches information of the type of call that has been executed in the data packet sent. The slave can thereafter take appropriate action.

The I^2C slaves have its unique address ranging in a sequence in the interval 1-127. The reason for having the addresses in a sequence was that when the master performs a broadcast, it also provides a number and if the slaves own address is a multiple of the attached number it follows the master instruction, otherwise the slave leaves the interrupt sub routine instantaneously.

7.8.2 Communication Between Microcontroller and Computer

All communication with the computer from the MCUs are made via the master MCU of the I^2C serial bus. The communication are made via UART (Universal Asynchronous Receiver/Transmitter) described in section 4.5, over USB interface to the computer.

There is a similar user defined high level protocol used for UART that was implemented for the I^2C bus, the protocol is defined in table 3. Since the master in the I^2C bus does not make any own calculations, nor store any new data, all messages sent to the master from the computer needs to be forwarded to the slaves in the I^2C bus.

Computer Call	**Master Action**
0: BROADCAST 1: Number	Make an I^2C broadcast to call all the slaves on the bus line. Forward the number as the second byte of data.
0: REQ_DISTANCE 1: SLAVE_ADDRESS	Ask the specific slave to send the latest calculated distance, thereafter forward it to the computer.
0: REQ_ADC_VALS 1: SLAVE_ADDRESS	Ask a specific slave to send the whole array of measurement data. Forward all of the measurement points to the computer.
0: SET_DIG_POT 1: SLAVE_ADDRESS 2: Value (0-127)	Request a specific slave to change value of the digital potentiometer. Call the slave address and forward the value. A mask is used (0x7F) to guarantee that the received value is allowed.

Table 3: *User implemented UART protocol for communication between computer and microcontroller. The microcontrollers action is described at each message from the computer. The communication consists of 3 bytes, index of each byte is written in the Computer Call-column. The words written in caps after the index are macrovalues defined both in the computer and the microcontroller*

The data packets sent from the computer to the master consists of 3 bytes. Refer to Table 3 for an explanation of the implemented features. When the expected amount of data has arrived via UART to the master module, an interrupt subroutine is called. In the subroutine the requested action from the computer is performed. The master forwards the message to the slave (or slaves, if the broadcast address is called) in the UART interrupt subroutine thereafter leaves the subroutine and waits for the slave to reply, if a reply is requested. When the slave replies with an answer, the master enters an I^2C interrupt subroutine and forwards the message to the computer.

There is no specific call from the computer to tell a slave to perform a ping, instead the broadcast address is used and the number provided is the slaves own address. This means that when the intended slave ensures that its unique address is a multiple of the number provided, that slave will be trigged, all other slaves that does not have a matching address leaves the interrupt subroutine instantly.

7.9 Programming Language and IDE

The Integrated Develop Environment (IDE) used for programming the Atmels MCU was Atmel Studio which is the development platform provided by Atmel.

To develop programs and program the Arduino, Arduinos development

tool Arduino Studio was used along with prewritten libraries for the peripheral hardware components that was connected to the microcontroller.

The project files for the final MCU used, the STM32F303RET6, were conducted in two steps. Initially, the project was generated in STM32 CubeMX, which is provided by STMicroelectronics. STM32CubeMx enables initialization of peripherals such as ADC, digital input/output ports, external oscillator, communications etc. STM32CubeMX also allows you to define the different parameters of the peripherals, for example the sampling rate and resolution of the ADC and the baudrate of the communication. This configuration is possible to do by changes in the registers on the MCU, but it is time saving to use STM32CubeMX for the task instead. Figure 37 shows a screenshot of the pinout configuration of STM32CubeMX.

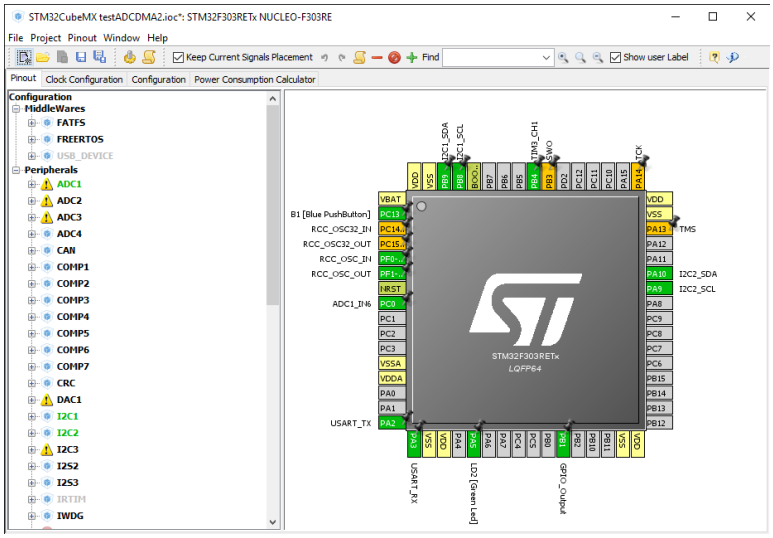

Figure 37: *Pinout configuration screen of STM32CubeMx, allows the user to add peripherals to the configuration. Pins marked as green are implemented in the program*

The IDE used to program the final STM32F303RET6 development boards was eclipse C/C++ with stm32 toolchain for GNU-ARM plugin. This plugin enabled programming and debugging of the microcontroller directly in eclipse.

All the program code for the microcontrollers has been written in C-code. The real time communication between the computers and microcontrollers are made via Matlab. Some of the initial communication and development of algorithms was written in C-code on the computer, apart from that all code running on computers in this project are written in Matlab.

8 Result

8.1 Arduino Rig and Road Finding Algorithm

The accuracy of each sensor is within the +/-3 mm margin of error that the manufacturer specified. When the sensors are placed 15 cm apart, the algorithm can find the road dummy but with insufficient precision. When the sensors are placed 10 cm apart the precision increased within the demand of 2 cm.

The algorithm used for detecting the road works as expected if and only if the measured data is of sufficient precision, smaller deviations from the actual value can be handled and the algorithm can still determine an accurate enough position. If a sensor detects an incorrect distance, such as a 2nd or 3rd echo, the algorithm does not work properly. It assumes the floor to be at the ground to be at the distance provided by the lowest sensor, and if that distance is double or triple the actual distance, the other distances will have an offset.

The algorithm was simulated with normal distributed values around 0 with a standard deviation of 4 mm to simulate measurement errors that are likely to occur on the test rig. 20 samples were tested and the the result can be seen in Figure 38. This can be put into comparison with the 8 mm standard deviation in Figure 39 which should be seen as the worst case scenario in this project.

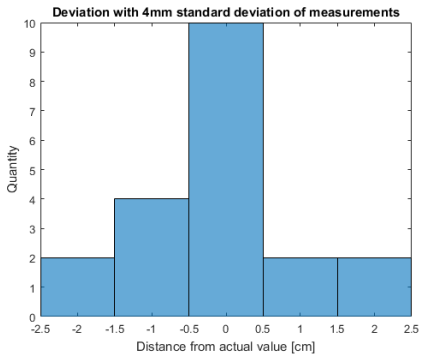

Figure 38: *4 mm standard deviation of measurements.*

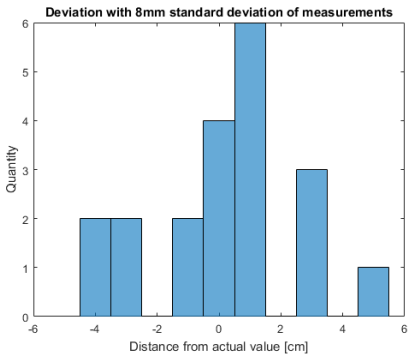

Figure 39: *8 mm standard deviation in measurements.*

The algorithm could most often handle the values and still pinpoint the correct position of the ERS elevation at 4 mm standard deviation, it could stay within the 20 mm deviation which is the acceptable error in the specification of this project. At the case for 8 mm deviation in Figure 39 the result is clearly insufficient for the project.

8.2 Sensors

Measurements proves that the sensors oscillation frequency is about 41 kHz, see Figure 40. Biltema's sensors compared to the sensors that was provided in the lab had a sensitivity which was significantly lower but since the transducers are made for the type of environment, these sensors were chosen.

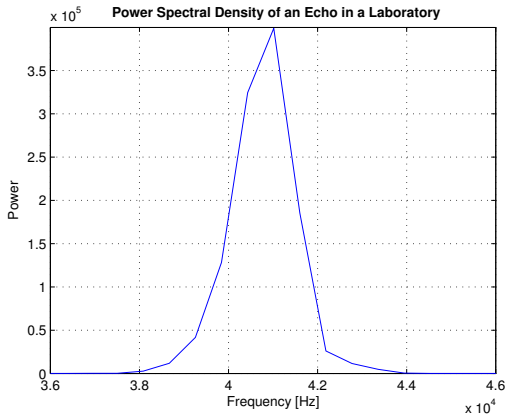

Figure 40: *Power spectral density of one of the ultrasonic transducers receiving an echo in laboratory environment.*

As can be seen in Figure 40, the bandwidth of the transducer is narrow. This is the echo received after an ultrasonic ping. Attempts has been made to alter the frequency of the emitting transducer, but with no notable difference with the analyzed power spectral density.

When sampling at 1.2 MHz the correlation with an ideal echo gives an accurate result in Matlab. The result is also repeatable, several pings provides the same result. However, when implementing the algorithm on the sensor modules, the sampling speed was reduced to 225 kHz due to lack of memory space in the MCU and also to decrease time for calculations. This led to increased deviation of the measured distances. The deviation between different measurements without changing the setup is up to 10 samples which translates to about 8 mm away from where the echo reflects.

8.3 Ultrasonic Positioning System

Attempts to ping all the sensors simultaneously is unsuccessful, the consequence is that the correlation method (described in Section 7.1.1) detects the distance value later than it occurs and thereby, the distance seemed to be further than it actually is. 3 ms is seen as the least time that is required to wait for a previous ping not to interfere with a new one, the time is estimated after tests i laboratory environments. Attempts were also made to

ping every second and third sensor in the array, but the result remains the same.

The time for the calculations using FFT, IFFT and locate the maximum value in the transformed array is 20 ms, this along with the CPUs gathering and compiling of the measurements should be able to meet the condition of an positioning update frequency of 30 Hz. However, since the transducer can not ping simultaneously. This means $6 * 3\ ms + 20\ ms = 38\ ms$ and this excludes the time for the CPU to gather and compile the measurements data from the slave modules. The final update frequency has not been tested but an adequate estimate is that it a new value could be provided every 50 ms since the road finding algorithm is a lot less processor intensive than the distance measurement.

8.4 Ultrasonic Modules

Attempts were made to use a wider bandwidth of the transducer, both by changing the frequency of the PWM signal and thereby see if another value could be detected. The result was not affected, the only change from when the PWM signal was using the 40 kHz signal is that the amplitude of the transmitted soundwave is significantly lower, and because of that, the returning echo is also lower in amplitude. Attempts were also conducted when the PWM frequency is set to counter-phase, in order to quicker stop the oscillation of the transducer. This did not work as intended, the result was only that the resonant circuit between the transducer and the transformer was attenuated, which also decreased the output amplitude significantly.

8.5 Noise and Other Unwanted Effects

The noise level of the measurements of ultrasonic echo is mainly affected by the cross-talk from the transmitting transducer. The cross-talk appears to consists of both electric and acoustic signals that are detected in the measurements. The mix of cross-talk seem to contain both a 40 kHz signal that most likely goes through the receiving transducer and a higher frequency. The crosstalk affects the first 10 cm of a measurement and it might interfere with the returning echo if the distance measured is small see Figure 41 for a visualization of the matter. The time axis in Figure 41 is represented by a distance in meter. The distance represents the space between the membrane of the transducer and the reflecting surface.

Apart from the crosstalk of the transducers there is either none detectable or very low noise. The noise level in a sample is generally between 1-3 discretion levels when 8 bit resolution is used in the ADC, the source for the noise is assumed to be the receiving transducers itself since the noise seem to have the same frequency as the transducers resonant frequency of roughly 40 kHz.

An unwanted effect could be seen with both the HC-SR04 distance sensor described in Section 7.2.2, and with the in-house built distance modules. The unwanted effect is that sometimes the direct path for the sound is attenuated more than other paths combined together. Since the HC-SR04 work with threshold detection, the first echo is not strong enough to exceed the threshold. The correlation algorithm yields the highest output with the echo that has greatest amplitude. Therefor, both the HC-SR04 and the correlation algorithm on the sensor modules provides inaccurate measurement data in this case. Since the transducers are mounted in housings with a flat surface, this creates a parallel surface with the ground where the sound can reflect between. Therefore, when the echo has a low amplitude in the direct path, the detected echo seems to be a second or even third reflection. Most of the double and triple reflections occurred when the sensors pinged at the road dummy and hit irregularities such as surface level difference and joints.

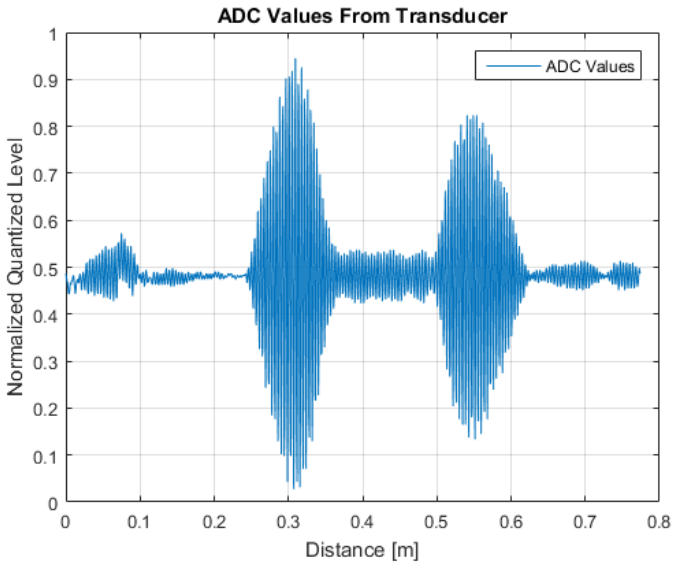

Figure 41: *8-bit ADC sampling at 225 kHz. The crosstalk in the beginning of a sampled echo is visual as the first peak between 0-0.1 m. The returned echo beginns at 0.24 m and the 3rd peak represents the double-echo.*

8.6 Tests Conducted on Road

Without any windbreak echoes are detectable by the algorithm up to a speed of 100 kmph see Figure 43, but with a notable attenuation of the echo above 80 kmph, Figure 42 shows the echo at 70 kmph and is still clearly detectable when the vehicle is moving in a velocity of 110 kmph and no windbreak on the transducer, there is no echo to be detected, see Figure 44, neither visible to the eye in the plot nor the algorithm. At velocities below 70 kmph, the

returning echo looks similar to the echo plotted in Figure 42.

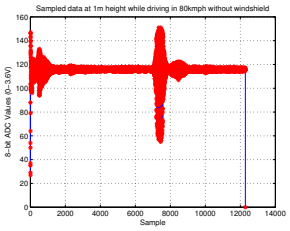

Figure 42: *A vehicle moving at 70 kmph.*

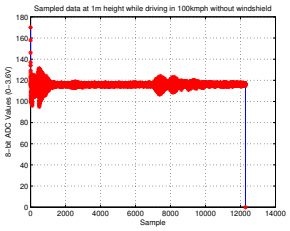

Figure 43: *A vehicle moving at 100 kmph.*

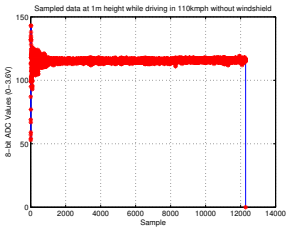

Figure 44: *A vehicle moving at 110 kmph.*

When adding either of the windbreaks, displayed in Figure 28 and Figure 29 echoes can easily be detected in 110 kmph. Both windbreaks gave a similar results with sufficient amplitude of the returning echo up to 110 kmph, see Figure 45, Figure 46 and Figure 47.

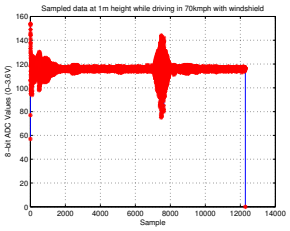

Figure 45: *A vehicle moving at 70 kmph.*

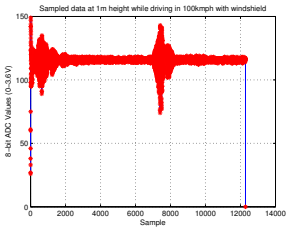

Figure 46: *A vehicle moving at 105 kmph.*

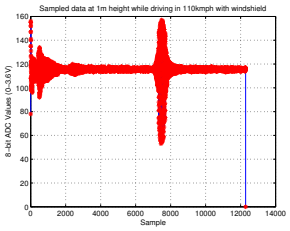

Figure 47: *A vehicle moving at 110 kmph.*

The tests show that the frequency content of the signal is not significantly affected due to Doppler effect. The tool *spectral analysis* in Matlab shows that the content of the sampled signal is the same no matter what the velocity of the vehicle where. At 0 kmph in Figure 48, the amplitude is lower than when the car is moving in 80 kmph and 110 kmph as seen in Figure 49 and Figure 50.

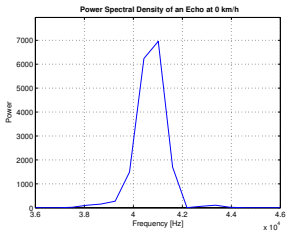

Figure 48: *A vehicle moving at 0 kmph.*

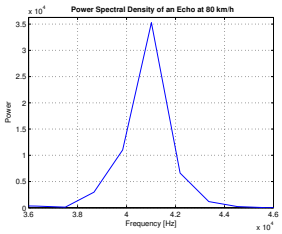

Figure 49: *A vehicle moving at 80 kmph.*

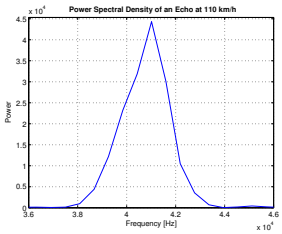

Figure 50: *A vehicle moving at 110 kmph.*

Since the frequency content was not changed while driving, the correlation algorithm was able to correlate with an ideal echo and give a clear result of the distance to the ground. Most measurements gave 98 cm as result, which also was the actual measured distance with a folding rule from the ground to the window of the car.

8.7 Costs During the Project

Price for the ultrasonic modules were roughly 500 SEK each in hardware costs see bill of materials in Appendix A. This price includes only component costs. The prices for cables and screws are not included since they are collected in the building and no price information is available, they are also relatively cheap.

The master modules cost is under 100 SEK, the cost is only the equivalent of a MCU, crystal and a USB connector. The USB connector should be excluded in a final design since the master module should handle all calculations instead of the computer that in the latest setup handles all the calculations.

The price for peripherals are limited to the price of the DIN rail and the cables connector combining the modules to each other. This cost is approximated to 200 SEK.

All in all, the final setup costs somewhere between 3,500-4,000 SEK. Spare parts remain to connect one additional transducer module and there are also spare parts to replace all of the components on the in-house manufactured shield in case any parts would stop working. If the extra transducer would be assembled, there are no spare shield, no spare MCU and no spare transducer.

The cost to order all the unused parts is less than 1,000 SEK. The storage works as an insurance, if any component breaks it can easily be replaced without waiting several days for a new delivery.

Other components bought during an early phase of the development includes assortment boxes to ease the warehousing of smaller components such as SMD resistors and capacitors. Arduino ultrasonic distance sensors

where also bought in an early phase to test out the algorithm, those costs 60 SEK each and 7 of them where used in the project. Meaning 420 SEK. The Biltema aftermarket back sensor kits were also bought in early. The only thing that was needed from the kits was the transducers, one kit costs 399 SEK which means that each transducer costs roughly 100 SEK. The price for other transducers as the ones found in the lab was about 50-150 SEK. This means that the cost for each transducer in the development process are reasonable. A roll of filament for the 3D printer were also purchased, this cost 299 SEK and this roll was enough for all the 3D prints throughout the project.

9 Discussion of Result

9.1 Arduino-Rig and Road Finding Algorithm

The main limitation with the Arduino test setup are the sensors, they are not robust enough for the final application and they are using transducers which are not sealed. A limitation with the visual feedback is the stepper motor which is not strong/fast enough to simulate the speed of the real rig and the Arduino stepper library which blocks the processor until the steps have been completed.

In the Arduino-rig, the program was implemented with a median filter which did a number of pings and used the median value of the distances. This filter was used to compensate the double echos that sometimes was misinterpreted as the returning echo. The filter did however not affect the result of the measurements, once the sensor recorded a secondary reflection, it was likely to do so again when a ping was sent to the same surface. Therefor this filter only caused unnecessary delays in the compiling of the measurement data and has been discarded. Since the double and triple reflections disrupted the algorithm, a paper is placed over the road dummy to smooth out the surface. This solution helps and reduces the amounts of occurrences of double reflections.

9.2 Sensors

Since the sensors has a resonance frequency of 41 kHz, the wavelength of the soundwave is 8.29 mm assuming sounds velocity in air to be 340 m/s. This distance seems to have a connection to the deviation of about 8 mm that correlation algorithm gives. When plotting the ideal echo together with the measured one it can be seen that the echoes differ in length and amplitude. This is probably due to the fact that the sound can travel different paths and thereby the form of the echo is changed. This is likely the error that the correlation algorithm gives, because the correlation matches the periods with maximum amplitude. Then assumes that the measured echo starts where the predefined echo start, which in fact can vary.

The measured echo and the ideal pre-sampled echo can be out of phase with each other, since the correlation matches the ideal echo over the measured echo this phase difference can give a maximum error one wavelength. This means that the correlation algorithm can only give a rough estimate of the actual distance and for more accurate value some additional method is needed.

The first idea with correlation was to use a point source as ideal echo recorded from a thin wire and only use the first periods of the echo. This because the first detected period should always look like a point source from any surface and thereby only correlate with the point source. This would have resolved the problem with different sized echoes since the correlation

would only match the beginning of the echo and therefor show a more correct result. Unfortunately, this does not seem to work, which could be because of the narrow-banded transducers, the few periods of the ideal echo are still about 41 kHz and correlates well with the middle part of the echo where the amplitude has its maximum.

Since the signal that is correlated is a sinusoidal, the correlated data will have both positive and negative peaks. Ideally the positive peaks should be where the two signals matches the best because where they are as most negative they are 180° out of phase. However since the error is about +/- 8 mm which relates to one wavelength, it could be beneficial to take the absolute values of the correlated data. This because the next peak will always be 8 mm away, but with the absolute value the next peak is only 4 mm away. This could yield a better result with only 4 mm deviation.

A study by IEEE [42] has been done where they have developed a recipe for robust high accurate ultrasonic range measurement system for piezoelectric transducer. They are also utilizing cross correlation for a rough estimate. And for increased precision and to refine the result from the cross-correlation estimate they take advantage from a phase-shift algorithm. However they are utilizing FHSS(Frequency Hop Spread Spectrum) because they use wide-banded microphones, which could be utilized in this project if there exists affordable cased widebanded microphones on the market. To be able to use the phase-shift algorithm the transmitted signal needs to be of FHSS type, where the phase-shift between the hops are measured, also the transmitted signal needs to be measured for comparison. It would also in this project be preferable to correlate with the transmitted signal instead of a recorded echo since this will make the system less sensitive for unexpected changes of parameters such as aging. FHSS and Frequency Modulation (FM) is no possibility for this project at this stage, it might be worth to test some kind of Amplitude modulation (AM) and validate if this would increase the accuracy. However since this project is looking into shorter distances there is a limit in time for the transmitted signal. It could also be possible to instead of using FHSS try and make a phase shift of 180° in the transmitted signal and see if it is detectable in the measured data.

It might be possible to widen the frequency response of the existing transducers and thereby possible to utilize FM/FHSS. According to another IEEE study [43], they succeeded to widen the bandwidth to 10-15 kHz. By adding an inductor and a resistance parallel to the transducer it is possible to add a second resonance peak which widens the frequency response of the transducer. This could be a possibility but needs to be tested. A bandwidth of 10-15 kHz is probably on the limit, especially because the amplitude is decreased with this circuit and the frequency response is at lowest at the ends of the interval. In the study the 40 kHz transducer that was tested yielded two resonance peaks at 36.5 kHz and 44 kHz with an inductance of 5 mH and resistance of 100 Ω. If the same circuitry could be applied to the

transmitter a frequency hop between these two resonance peaks would be possible.

Other possibilities are threshold detection or maybe correlation of the derivative of the envelope. Another solution could be to make a lot of ideal echoes and take the average one for the correlation algorithm which would hopefully yield more robustness instead of the present 8 mm deviation. This accuracy of +/-4 mm has been proven to work with the Arduino rig in ideal environment, so if the sensors are robust enough to have at least the same accuracy in real environment, it would probably work. There has not been any part of the projects that looks in to the opportunity to use threshold detection sensors in the final prototype, but when mounted under a vehicle the performance would probably be affected due to the noise under a moving vehicle, both electric noise and wind that passes the membrane, which could trig the detector.

9.3 Noise and Other Unwanted Effects

The noise seems to be of small problem for the algorithms. The electrical cross-talk is unwanted and measures has been taken to minimize it. The transducer use shielded cables and the connectors to the PCB from the cables have been shielded with aluminium. The PCB has ground planes on both sides. Still some minimum electrical crosstalk can be seen and there could be more changes to reduce it. It is unknown if the transducers are electrically shielded, so a possibility could be to try and electrically shield them as well. One other possibility would be to power the ping circuit of the slave modules from an additional power supply to get rid of the induced disturbances from the inductive transformer.

The acoustic cross hearing is unwanted when correlating with a predefined echo, but could prove useful if auto-correlation would be used. The auto-correlation was also attempted where the cross hearing is used as the ideal echo. Advantages with this method is that regardless of changes that could alter the transducers properties such as aging, the auto-correlation will always work whereas the predefined echo will not. To minimize the acoustic crosstalk, a screen can be placed between the transmitting and receiving side.

The cross-correlation yields peaks at every detected echo, with the largest peak for the echo with greatest amplitude. A solution to the problem with attenuation of the direct acoustic path is to look for the earliest peak instead of the peak with greatest amplitude. This could be done by first finding the highest peak, thereafter multiplying this value with a constant < 1 that is experimentally established so that the value is above the noise floor but low enough to find earliest peak and then backtrack to find it. [42]

9.4 Ultrasonic Positioning System

In this project, the array of sensors is considered completely parallel with the roadway. However, in future applications it should be taken into consideration that the array of sensors is not completely parallel relative the roadway due to the inclination of the roadway and also due to tilt of the vehicle.

9.5 Test Conducted on Road

Since the transducers were placed on a stick that was held outside the window by a human and not fixed into a stationary position there is an uncertainty to the measurements. Sometimes echoes at higher speeds had greater amplitude and a more clear result as compared to measurements in lower speed. This is likely because the stick or ground is at an angle. Therefor it is possible that speed over 100 kmph still could be detectable without a windbreak. However, the result that a windbreak gave better result is indisputable. Since the transducers were placed at roughly 1 m above ground the signal will be more attenuated than if the transducer would be placed at a distance of 20 cm. The impact of this could be that a windbreak is not needed at all, even though the windbreak helped. More repeated tests are needed to be conducted while driving and instead place the transducers beneath the car at a fixed position where they actually should be.

A factor that might have increased the detectability of the returning echo could have been to increase the gain of the op amps. This was held relatively low due to the problems of the bias currents discussed in Section 7.7.1.

The Doppler effect did not seem to affect the sampled values, this can be concluded by looking at Figure 48, Figure 49 and Figure 50. The lack of interference from the Doppler effect could be because the receiving transducers bandwidth is narrow and it can only resonate to give a detectable signal in a small spectrum. Also the fact that the sound is emitted perpendicular to the direction of travel should minimize the Doppler effect. When the ultrasonic ping has traveled 2 m, which is equivalent to the distance from the sensor to the ground and back, the car has moved 22 cm when travels at 110 kmph and assuming the sound velocity in air to be 340 m/s.

9.6 Costs During the Project

The development costs for the project seems to be reasonable. Since the development cost for one sensor unit was just above 500 SEK. The price could be lowered if components were ordered in larger quantities and if only one, more powerful MCU were used, and thereby eliminate the need for such powerful MCU in every slave module. Also by ordering the transducer

directly from the supplier or by using equivalent more affordable transducers, this price would go down drastically if it comes to a manufacturing process.

One other way to go would be to keep the MCUs on each of the slave modules and use the integrated op amps instead. Those are sufficient for amplifying a 40 kHz signal 100 times for each amplifier, this was determined after measurements on them. The internal op amps were however only tested and not implemented in a circuit due to the risk that if a too high voltage were to reach them, the whole MCU might have to be discarded. An MCU costs 6 times the price of an op amp and by using the PCB-shield, the conductors could be kept as short as possible to avoid electromagnetic interference. Therefor, it was not a solution for this evaluation project but might be of interest if a similar set-up is used in the future in a more completed state.

It could also be possible to use only one op amp stage instead of two, using one single op amp with a wider bandwidth which could reduce the complexity of the circuit and possibly also reduce the cost.

9.7 Topics for Future Work

9.7.1 Absolute value of the correlated data

By taking the absolute value of the correlated data it could be possible to reduce the error as described in Section 9.2. This is a easy and quick test to do which should be the first thing to test before other more complicated methods.

9.7.2 Change the Emitted Signal to Counter Phase

In an attempt to obtain a better result when correlating, the pulse that triggers the transmitting transducer could after half of the periods in the ping signal, be delayed half a period to get a phase shift in the transmitted signal. This phase shift should then be detectable in the received signal.

9.7.3 Use Microphone or Increase Bandwidth of Transducers

The emitting transducer can be forced to emit ultrasonic sound in a different frequency much easier than the receiving transducer can detect another frequency. Therefore, by looking into the possibility to use a microphone that can record ultrasonic sound, it might still be possible to use a piezoelectric transducer for emitting sounds. Microphones such as underwater sonars already exists, but the cost and availability of those has not been investigated during this project.

Another alternative would be to attempt to increase the bandwidth of the existing transducers to be able to use the advantages with FM/FHSS as described in Section 9.2.

9.7.4 Amplitude Modulation

Another attempt to change the emitting signal could be to change the amplitude, for example by either changing the quantity of PWM pulses, or by changing the frequency of the PWM signal that triggers the transducer.

9.7.5 Add Hardware Support for Envelope

For the next version an envelope detector could be added to the hardware and connected to an ADC channel. If it is concluded that it is useful.

9.7.6 Safety Detection System

Another topic could be to look in to the possibility to use the ultrasonic transducer as a safety system that detects if an object reaches between the wheels of the vehicle. The charging could then be interrupted instantly if a hand or an animal comes close to the power transfer between the sliding contact and the conductor on the roadway.

9.7.7 Effects on animals of 40 kHz ultrasound

A lot of different animals can hear in the ultrasound range, example Table 1. Therefor it could be useful to conduct a study how ultrasound affects animals and what effects it would have if every vehicle would use the UPS.

References

[1] S. Riksdag, "Klimatfärdplan 2050 - strategi för hur visionen att sverige år 2050 inte har några nettoutsläpp av v"axthusgaser ska uppnås," http://www.riksdagen.se/sv/dokument-lagar/dokument/kommittedirektiv/klimatfardplan-2050—strategi-for-hur-visionen_H2B153, visited: 2016-06-09.

[2] Elonroad, "Elonroad," http://elonroad.com/, visited: 2016-06-15.

[3] Siemens, "ehighway - eldriven godstransport pålandsväg," http://w3.siemens.se/mobility/se/sv/interurban_mobility/road_solutions/ehighways-eldriven-godstransport-pa-landsvag/pages/ehighways-eldriven-godstransport-pa-landsvag.aspx, visited: 2016-02-23.

[4] L. Nohrstedt, "Sverige kan bli först med allmän elväg," http://www.nyteknik.se/nyheter/bygg/byggartiklar/article3929682.ece , visited: 2016-02-23.

[5] Siemens, "ehighway-picture," http://w3.siemens.se/mobility/se/sv/interurban_mobility/road_solutions/eHighways-Eldriven-godstransport-pa-landsvag/PublishingImages/20131120_eHighway_SCANIA-tr-highres_2.jpg, permission to publish the picture has been permitted 2016-06-09 by Anders Bylund at Siemens.

[6] Elways, "Elways test track," http://elways.se/testresultat-arlanda/ , visited: 2016-02-23.

[7] ElwaysPicture, "Picture of elways test track," http://elways.se/wp-content/uploads/2011/10/Bild1-300x169.png , permission to publish the picture has been permitted 2016-06-10 by Gunnar Asplund at Elways.

[8] volvo, "The road of tomorrow is electric," http://news.volvogroup.com/2013/05/23/the-road-of-tomorrow-is-electric/, visited: 2016-02-23.

[9] J. M. R. H. L. G. J. P. J.-A. Dahlström, "Ne uppslagsverk, ultraljud," http://www.ne.se/uppslagsverk/encyklopedi/lång/ultraljud, visited: 2016-05-23.

[10] D. J. Woo, "A short history of the development of ultrasound in obstetrics and gynecology," http://www.ob-ultrasound.net/history1.html, visited: 2016-01-20.

[11] Brittanica, "Elastic wave," http://global.britannica.com/science/elastic-wave, visited: 2016-01-23.

[12] P. A. Tipler and G. Mosca, *Physics For Scientists and Engineers*, 6th ed. W. H. Freeman and Company, 2008.

[13] D. Ensminger and L. J. Bond, *Ultrasonics Fundamentals, Technologies, and Applications.* Taylor & Francis Group, 2011.

[14] J. Baun, *Principles of General & Vascular Sonography.* Self Published, 2009.

[15] A. A. Vives, *Piezoelectric Transducers and Applications.* Springer, 2008.

[16] G. Lindstedt, "Borrowing the bat's ear for automation - ultrasonic measurements in an industrial environment," Ph.D. dissertation, Lund University, Faculty of Engineering, 1996.

[17] NDT, "Piezoelectric transducers," https://www.nde-ed.org/EducationResources/CommunityCollege/Ultrasonics/EquipmentTrans/piezotransducers.htm, visited: 2016-01-25.

[18] MartinLogan, "Esl 101: Electrostatic theory," http://www.martinlogan.com/learn/electrostatic-speakers.php, visited: 2016-05-26.

[19] A. Carovac, F. Smajlovic, and D. Junuzovic, "Application of ultrasound in medicine," *Acta Informatica Medica*, 2011, faculty of health sciences, University of Sarajevo.

[20] G. Jones and M. W. Holderied, "Bat echolocation calls: adaptation and convergent evolution," https://www.ncbi.nlm.nih.gov/pmc/articles/PMC1919403/, visited: 2016-02-01.

[21] LSU, "How well do dogs and other animals hear?" http://www.lsu.edu/deafness/HearingRange.html, visited: 2016-05-28.

[22] C. S. B. Michael T. Heideman, Don H. Johnson, "Gauss and the history of the fast fourier transform," *IEEE*, vol. 1, no. 4, 1984.

[23] Wolfram, "Fast fourier transform," http://mathworld.wolfram.com/FastFourierTransform.html, visited: 2016-05-25.

[24] D. K. MASLEN and D. N. ROCKMORE, "The cooleytukey fft and group theory," *MSRI Publications*, vol. 46, 2003, http://library.msri.org/books/Book46/files/11maslen.pdf, visited: 2016-05-25.

[25] G. Wolberg, "Fast fourier transforms: A review," Department of Computer Science Columbia University, New York, NY 10027, Tech. Rep., September 1988, https://www.google.se/url?sa=t&rct=j&q=&esrc=s&source=web&cd=9&ved=0ahUKEwigrN6jy5rNAhVLb5oKHaF9AysQFghhMAg&url=http%3A%2F%2Facademiccommons.columbia.edu%2Fdownload%2Ffedora_content%2Fdownload%2Fac%3A142809%2FCONTENT%2Fcucs-388-88.pdf&usg=AFQjCNG1ZM-clNbWUe-mewZdBe9RggBHtQ&sig2=QFoAcfSIav3-IxMsyNHBiA&cad=rja.

[26] J. Fessler, "Eecs 451 digital signal processing and analysis lecture notes," http://web.eecs.umich.edu/ fessler/course/451/l/pdf/c6.pdf, visited: 2016-05-26.

[27] A. D. Linear, *Linear Circuit Design Handbook*. Newnes, 2006, edited by Hank Zumbahlen, 2008, http://www.analog.com/library/analogDialogue/archives/43-09/linear_circuit_design_handbook.html.

[28] A. D. Data, *Data Conversion Handbook*. Newnes, 2005, edited by Walt Kester, http://www.analog.com/en/education/education-library/data-conversion-handbook.html.

[29] T. D. Limited, "Jitter effects on analog to digital and digital to analog converters," http://www.thewelltemperedcomputer.com/Lib/Troisi.pdf, visited: 2016-05-22.

[30] T. Phase, "I2c background," http://www.totalphase.com/support/articles/200349156-I2C-Background, visited: 2016-06-02.

[31] P. Semiconductor, *I^2C-bus compatible ICs*. Philips, 1988.

[32] N. Semiconductors, *UM10204, I^2C-bus specification and user manual*, 6th ed., NXP Semiconductors, april 2014, http://www.nxp.com/documents/user_manual/UM10204.pdf.

[33] T. Instruments, "Keystone architecture universal asynchronous receiver/transmitter (uart)," http://www.ti.com.cn/cn/lit/ug/sprugp1/sprugp1.pdf, visited: 2016-05-31.

[34] B. Carter and T. R. Brown, "Handbook of operational amplifier," http://www.ti.com/lit/an/sboa092a/sboa092a.pdf, visited: 2016-06-04.

[35] Arduino, "Arduino mega 2560," https://www.arduino.cc/en/Main/arduinoBoardMega2560, visited: 2016-03-17.

[36] ArduinoPicture, "Arduino mega 2560 picture," https://www.pololu.com/picture/view/0J3807, visited: 2016-03-17.

[37] C. Technologies, "Users manual v1.0 may 2013," https://docs.google.com/document/d/1Y-yZnNhMYy7rwhAgyL_pfa39RsB-x2qR4vP8saG73rE/edit, visited: 2016-03-17.

[38] Elecfreaks, "Hc-sr04 distance sensor picture," http://www.elecfreaks.com/store/images/Sensor_ObjDec_Ultra_HC_SR04_7.jpg, visited: 2016-03-17.

[39] diyspacepk, "Lm298 dual h-bridge module picture," http://diyspacepk.com/wp-content/uploads/2016/02/LM298-Motor-Driver-Breakout-1-600x600.jpg, visited: 2016-03-19.

[40] STMelectronicsPicture, "Stm32f303ret6," http://se.farnell.com/productimages/standard/en_GB/2424210-40.jpg, visited: 2016-06-03.

[41] STMelectronics, "Stm32f303xd stm32f303xe datasheet," http://www.st.com/content/ccc/resource/technical/document/datasheet/2c/6f/d7/64/1f/a3/4f/c9/DM00118585.pdf/files/DM00118585.pdf/jcr:content/translations/en.DM00118585.pdf, visited: 2016-06-03.

[42] C. J. B. M. M. Saad and S. Dobson, "Robust high-accuracy ultrasonic range measurement system," *IEEE*, vol. 60, no. 10, 2011.

[43] C. B. J.R. Gonzalez, "Low cost, wideband ultrasonic transmitter andreceiver for array signal processing applications," *IEEE*, vol. 11, no. 5, 2011.

Appendices

A Bill of Material

Table 4 shows the list of components used for every ultrasonic sensor module. In addition to the components listed below screws, nuts, pins and soldering tin were used, these were provided by the department and the cost for it seemed negligible. A 150 cm DIN rail and a 150 cm of shielded 9-conductor wire were used, these were excluded from the calculation since this is not considered as parts of the sensor modules.

3D Filament	A: 87484 D: 299[1]	B: Kjell & co E: 1	C:Velleman F: 1.75 mm in diameter, PLA filament. 300 m
Capacitor	A: - D: -	B: - E: 3	C: - F: 50 V 10 F electrolyte
Copper Laminate	A: - D: -	B: - E: 1	C: - F: Double sided
Dig. Potentiometer	A: TPL0401A D: 9.67	B: DigiKey E: 1	C: Texas Instruments F: 0-10 kΩ 127 steps
DIN Rail Clip	A: - D: -	B: - E: 1	C: - F: Metal
D-SUB9 Female	A: 171-009-203L001 D: 6.38	B: DigiKey E: 2	C: Norcomp Inc. F: Female Connector
D-SUB9 Male	A: 171-009-102L001 D: 5.96	B: DigiKey E: 2	C: Norcomp Inc. F: Male Connector
Microcontroller	A: STM32F303RET6 D: 91.66	B: DigiKey E: 1	C: STMmicroelectronics F: Nucleo Developmentboard
Op amp	A: LTC6240CS5 D: 14.88	B: DigiKey E: 2	C: Linear Technology F:
Crystal	A: ATS080B D: 2.50	B: DigiKey E: 1	C: CTS-Frequency,Controls F: 8 MHz
Reference Voltage	A: REF2033AIDDCT D: 29.61	B: Digikey E: 1	C: Texas Instruments F: Output: 1.65 V and,3.3 V
SMD Capacitor	A: Multiple D: 0.5 (typ.)	B: DigiKey E: 12	C: Multiple F: Several types. 6.8-10 μF
SMD Diode	A: LL4148 D: 0.64	B: DigiKey E: 2	C: Fairchild F:
SMD LED	A: LB,Q39G-L2OO-35-1 D: 2.11	B: DigiKey E: 1	C: OSRAM Opto F: Blue, 6 mA
SMD Resistor	A: Multiple D: 0.5	B: DigiKey E: 13	C: Multiple F: Several, 0-2 MΩ
Transducer	A: 43-137 D: 99.75	B: Biltema E: 2	C: Biltema F: Cased Transducers
Transformer	A: K4000001 D: 11.99	B: Farnell E: 1	C: Prowave F: 10:1 ratio, 10.6 mH, 40 kHz

Table 4: *Bill of material for each ultrasonic measurement module. A: Product number. B:Vendor. C: Manufacturer. D: Unit price (SEK). E: Units used per ultrasonic module. F: Comments*

[1] The price is for the entire roll of 340 m filament, 12.1 m is used for a box and 5.3 for a lid.

B Settings STM32CubeMx

Listed in 5 the settings for the microcontrollers peripherals are found. The settings regarding ADC, DMA, I^2C1, TIM1 and TIM3 are exclusively for the slave modulse whereas the USART is for the master module. I^2C2 is common for both devices.

ADC	Resolution	8 bit
	Scan conversion Mode	Disabled
DMA	Direction	Peripheral to memory
	Mode	Normal
	Increment address	Memory
	Data width	Byte
GPIO	PA2	USART2_TX
	PA3	USART2_RX
	PA5	LED
	PA9	I2C2_SCL
	PA10	I2C2_SDA
	PB4	TIM3
	PB8	I2C1_SCL
	PB9	I2C1_SDA
	PC0	ADC1
	PF0	RCC_OSC_IN
	PF1	RCC_OSC_OUT
I^2C1	I2C speed [kHz]	100
I^2C2	I2C speed [kHz]	100
	General Call address	Enabled
	Primary slave address	Unique
TIM1	Counter Period [ticks]	28 800
TIM3	Mode	PWM mode 1
	Counter Period [ticks]	1800
USART2	Mode	Asynchronous
	Baud rate [bps]	115 200
	Word Length	8 bit
	Parity	none
	Stop bits	1

Table 5: *The configurations for the different functions implemented on the MCU. The settings above lists only the settings changed from default.*

C Circuit Diagram of Shield

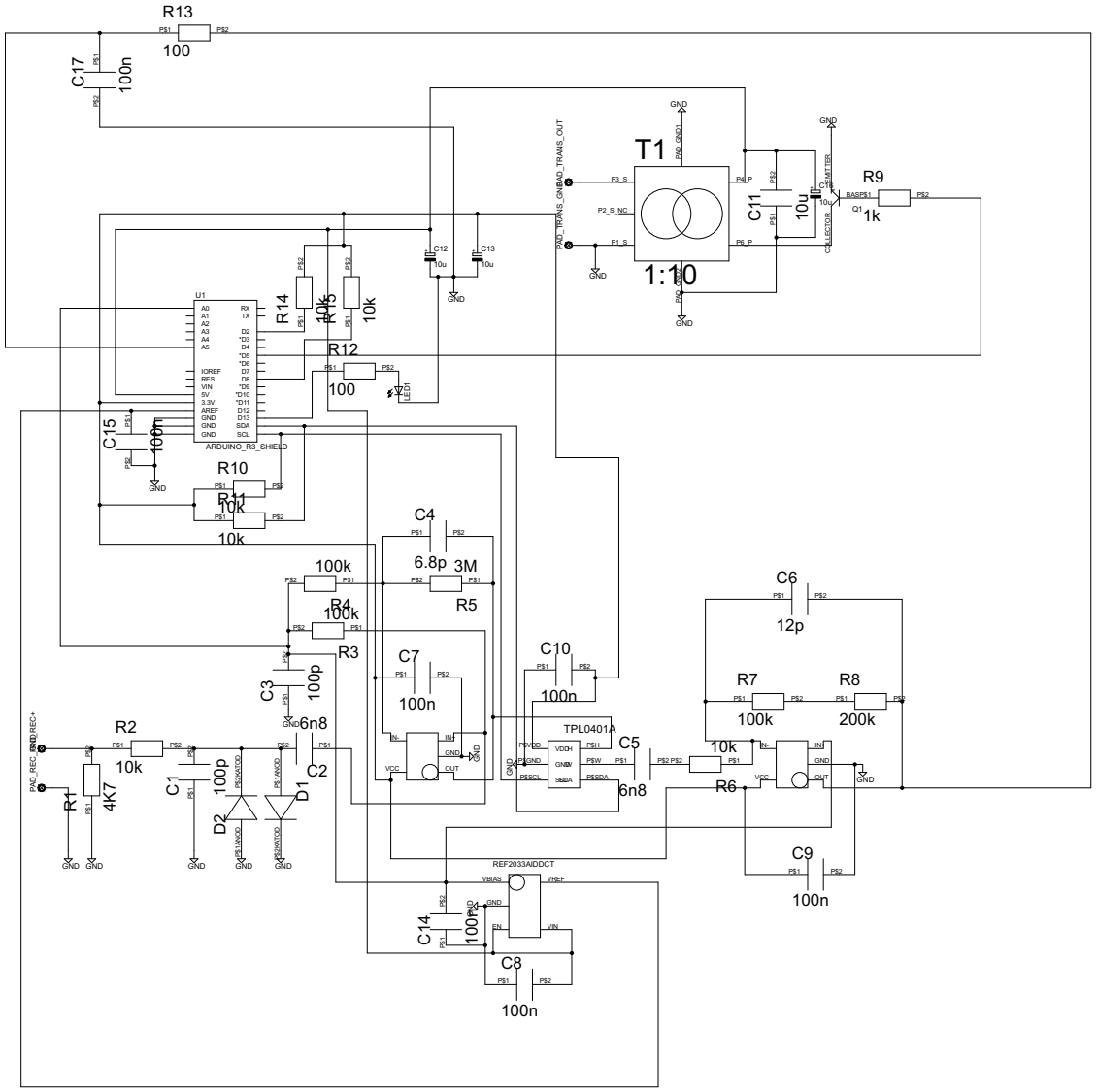

Part	Value	Device	Package	Description	SPICETYPE
C1	100p	SMD_CAP3.2X1.6	SMD_CAP3.2X1.6		
C2	6n8	SMD_CAP3.2X1.6	SMD_CAP3.2X1.6		
C3	100p	SMD_CAP3.2X1.6	SMD_CAP3.2X1.6		
C4	6.8p	SMD_CAP3.2X1.6	SMD_CAP3.2X1.6		
C5	6n8	SMD_CAP3.2X1.6	SMD_CAP3.2X1.6		
C6	12p	SMD_CAP3.2X1.6	SMD_CAP3.2X1.6		
C7	100n	SMD_CAP3.2X1.6	SMD_CAP3.2X1.6		
C8	100n	SMD_CAP3.2X1.6	SMD_CAP3.2X1.6		
C9	100n	SMD_CAP3.2X1.6	SMD_CAP3.2X1.6		
C10	100n	SMD_CAP3.2X1.6	SMD_CAP3.2X1.6		
C11	10u	SMD_CAP3.2X1.6	SMD_CAP3.2X1.6		
C12	10u	CPOL-EUSANYO_C'	SANYO-OSCON_C'	POLARIZED CAPACITOR, European symbol	
C13	10u	CPOL-EUSANYO_C'	SANYO-OSCON_C'	POLARIZED CAPACITOR, European symbol	
C14	100n	SMD_CAP3.2X1.6	SMD_CAP3.2X1.6		
C15	100n	SMD_CAP3.2X1.6	SMD_CAP3.2X1.6		
C16	10u	CPOL-EUSANYO_C'	SANYO-OSCON_C'	POLARIZED CAPACITOR, European symbol	
C17	100n	SMD_CAP3.2X1.6	SMD_CAP3.2X1.6		
D1	SMD_DIODE3.3X1.4	SMD_DIODE3.3X1.4	SMD_DIODE3.3X1.4		
D2	SMD_DIODE3.3X1.4	SMD_DIODE3.3X1.4	SMD_DIODE3.3X1.4		
LED1		LED_ESML0603	LED_SML0603		LED
			NONE	D	diode
PAD_REC+	LSP10	LSP10	LSP10	SOLDER PAD drill 1.0 mm, distributor Buerklin, 12H555	
PAD_REC_GND	LSP10	LSP10	LSP10	SOLDER PAD drill 1.0 mm, distributor Buerklin, 12H555	

Figure 52: *Bill of material for the circuit diagram*

PAD_TRANS_GND	LSP10 SOLDER PAD drill 1.0 mm, distributor Buerklin, 12H555	LSP10	LSP10
PAD_TRANS_OUT	LSP10 SOLDER PAD drill 1.0 mm, distributor Buerklin, 12H555	LSP10	LSP10
Q1	S8050	S8050	S8050
R1	4K7	SMD_RES3.2X1.6	SMD_RES3.2X1.6
R2	10k	SMD_RES3.2X1.6	SMD_RES3.2X1.6
R3	100k	SMD_RES3.2X1.6	SMD_RES3.2X1.6
R4	100k	SMD_RES3.2X1.6	SMD_RES3.2X1.6
R5	3M	SMD_RES3.2X1.6	SMD_RES3.2X1.6
R6	10k	SMD_RES3.2X1.6	SMD_RES3.2X1.6
R7	100k	SMD_RES3.2X1.6	SMD_RES3.2X1.6
R8	200k	SMD_RES3.2X1.6	SMD_RES3.2X1.6
R9	1k	SMD_RES3.2X1.6	SMD_RES3.2X1.6
R10	10k	SMD_RES3.2X1.6	SMD_RES3.2X1.6
R11	10k	SMD_RES3.2X1.6	SMD_RES3.2X1.6
R12	100	SMD_RES3.2X1.6	SMD_RES3.2X1.6
R13	100	SMD_RES3.2X1.6	SMD_RES3.2X1.6
R14	100	SMD_RES3.2X1.6	SMD_RES3.2X1.6
R15	100	SMD_RES3.2X1.6	SMD_RES3.2X1.6
T1	1:10	PROWAVE_K_TRANSFORMER	PROWAVE_K_TRANSFORMER
TPL0401A1	TPL0401A	TPL0401A	TPL0401A
U$1	LTC6240	LTC6240	LTC6240
U$2	LTC6240	LTC6240	LTC6240
U$3	REF2033AIDDCT	REF2033AIDDCT	REF2033AIDDCT

Figure 53: *Continuation of the bill of material for the circuit diagram*